Heliyon 10 (2024) e34980

Contents lists available at ScienceDirect

Heliyon

journal homepage: www.cell.com/heliyon

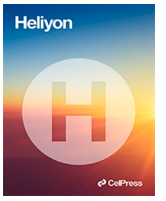

Research article

Synthesis of 2-aminothiazole sulfonamides as potent biological agents: Synthesis, structural investigations and docking studies

Syeda Khair-ul-Bariyah [a], Muhammad Sarfraz [b], Muhammad Arshad [b], Amir Waseem [c], Hidayat Ullah Khan [d], Shahnaz Khan [d], Ahsan Sharif [a], Zahoor Hussain Farooqi [a], Ejaz Ahmed [a,*]

[a] School of Chemistry, University of the Punjab, 54590, Pakistan
[b] Institute of Chemistry, The Islamia University of Bahawalpur, Bahawalpur, 63100, Pakistan
[c] Department of Chemistry, Quaid-i-Azam University, Islamabad, Pakistan
[d] Department of Chemistry, University of Science and Technology, Bannu, 28100, Pakistan

ARTICLE INFO

Keywords:
2-Aminothiazole
α-amylase
Antioxidant
Anti-Urease
α-glucosidase
NMR

ABSTRACT

A simplified synthetic approach involving sulfonylation followed by amino group alkylation produced new 2-aminothiazole derivatives. UV/Vis, infrared, and NMR spectroscopies confirmed their structures. Compounds **36**, **22**, **34**, and **35** showed strong inhibition against Jack bean and Bacillus Pasteurii urease, with IC_{50} values from 14.06 to 20.21 μM/mL. Compounds **20**, **26**, **21**, **29**, **30**, **31**, and **32** exhibited potent inhibitory effects against α-glucosidase and α-amylase, with IC_{50} values between 20.34 and 37.20 μM/mL. Compounds **33**, **26**, and **27** demonstrated potent DPPH scavenging, with IC_{50} values around 34.4–39.2 μM/mL. FMO analysis showed compounds **21**, **22**, **24**, and **25** having parallel aromatic ring systems due to π cloud interactions, while compounds **32** and **38** had distinct electronic density distributions. Compound **22** had HOMO and LUMO energy gaps of 5.805 eV, with bromo and fluoro substitutions in compounds **21** and **24** slightly increasing the gaps to 6.089 eV and 6.078 eV, respectively. Nitro groups in compounds **25** and **32** reduced the gaps to 0.384 eV and 1.187 eV. All compounds demonstrated high gastrointestinal absorption, non-permeability to the blood-brain barrier, and optimal skin permeation (Log Kp between −5.83 and −6.54 cm/s). Compounds **22**, **24**, and **38** had promising QED scores of 0.719, 0.707, and 0.860, respectively, with synthetic accessibility scores from 2.057 to 2.517. ADMET predictions indicated minimal toxicity, cardiovascular safety, and significant inhibitory potential for CYP enzymes. Strong in silico binding affinities (binding energies −5.75 to −7.63 kcal/mol) and metabolic stability suggest these derivatives are promising candidates for further drug development.

1. Introduction

The study of heterocyclic compounds is the most intricate and exciting field of organic science because of its physiological and industrial significance, voluminous theoretical research, and challenging synthetic procedures. Heterocyclic compounds are widely studied due to the large number of medications, dyes, natural products (alkaloids, vitamins, and antibiotics), and other molecules like

* Corresponding author.
E-mail address: ejaz.ahmed.chem@pu.edu.pk (E. Ahmed).

https://doi.org/10.1016/j.heliyon.2024.e34980
Received 8 May 2024; Received in revised form 18 July 2024; Accepted 19 July 2024
Available online 20 July 2024

nucleic acids that are closely linked to the development of life. The nitrogen-containing compounds are thought to be the most important heterocyclic compounds as a result of these considerations [1,2].

Aminothiazole nuclei and their many variants have long been employed as precursors in the synthesis of physiologically active drugs [3]. In medicinal chemistry and drug development research, the 2-aminothiazole scaffold has shown great promise due to its wide range of pharmacological applications [4]. 2-Aminothiazole is a common heterocyclic amine that is used as an intermediate in the synthesis of several compounds, such as biocides, fungicides, dyes, antibiotics, and chemical reaction accelerators. Numerous 2-aminothiazoles are altered with various groups for use in medicine [5–7]. Additionally, many 2-aminothiazole analogs' strong and targeted nanomolar inhibitory action is demonstrated in vitro anticancer evaluation tests against a variety of human malignant cell lines, including those from the breast, leukemia, lung, colon, CNS, melanoma, ovarian, renal, and prostate [8–10]. Biologists are still interested in these derivatives because of their wide range of applications in the administration of biological systems.

Several studies have explored the use of these substances for their antimicrobial [11–13], antifungal [14], anti-inflammatory [14], anesthetic [5], antiviral [7], anti-leukemic [15], and antiproliferative properties [16]. These substances have shown activity against various cell lines and enzymes related to eicosanoid metabolism [17,18].In medicinal chemistry, enzyme inhibition is key to developing new therapies for various diseases [19–21].

Alpha-glucosidase inhibitors, oral diabetes medications derived from microbes, delay carbohydrate absorption in the gut to reduce postprandial hyperglycemia and improve cardiovascular health [22].Alpha amylase and alpha glucosidase are key enzymes in carbohydrate breakdown, aiding intestinal absorption. They are targets for developing diabetes treatments [23].

Free radical species, with an odd number of electrons in their outer shells, are extremely unstable and constantly seek an electron to achieve stability [24]. Free radicals, created in mitochondria during oxygen metabolism, must be eliminated to prevent illnesses like infections, brain tumors, heart disease, diabetes, aging, and AIDS [25]. The development of antioxidant drugs has shown biological responses to infections through methods like chelating metal ions, dissolving peroxides, regulating hydrogen metabolism, preventing chain initiation, and scavenging radicals. These drugs are used in various medications to treat free radical-induced illnesses [26,27].

Urea amidohydrolase (E.C. 3.5.1.5), a hyperactive urease enzyme dependent on nickel (Ni), is a member of the phosphotriesterase and amidohydrolase family [28]. It is produced by various microorganisms, including soil bacteria, algae, plants, fungi, and invertebrates [29]. The urease enzyme quickly converts urea into ammonia (NH_3) and carbamic acid, which then becomes carbon dioxide (CO_2) and another ammonia molecule [30]. Excess ammonia from overexpressed urease kills human cells, leading to various diseases. These include urinary stones, urolithiasis, hepatic encephalopathy, pyelonephritis, hepatic coma, and urinary catheter encrustation [31]. Helicobacter pylori's urease enzyme allows it to survive in the stomach's low pH, potentially causing gastric and peptic ulcers [32,33]. Stomach cancer ranks second in global cancer deaths and fourth in frequency [34,35]. Excessive urease activity from urea fertilization leads to high ammonia levels, harming both environment and economy. This causes nutrient deficiency, ammonia toxicity, and raised soil pH, impacting plant growth [36].

Here, we present the synthesis and structural characteristics of 2-aminothiazole analogs as urease, α-glucosidase, and α-amylase inhibitors as well as antioxidant agents. Nine out of the twenty-one compounds are of novel origin. These compounds have exciting potential for controlling enzymes, which is important in medicine. We make these compounds more reactive and flexible using a two-step process that involves careful chemical changes. Alkylating sulfonamides improves their potency, bioavailability, and duration of action, among other pharmacological characteristics. Sulfonamides undergo alkylation, which modifies their chemical structure and

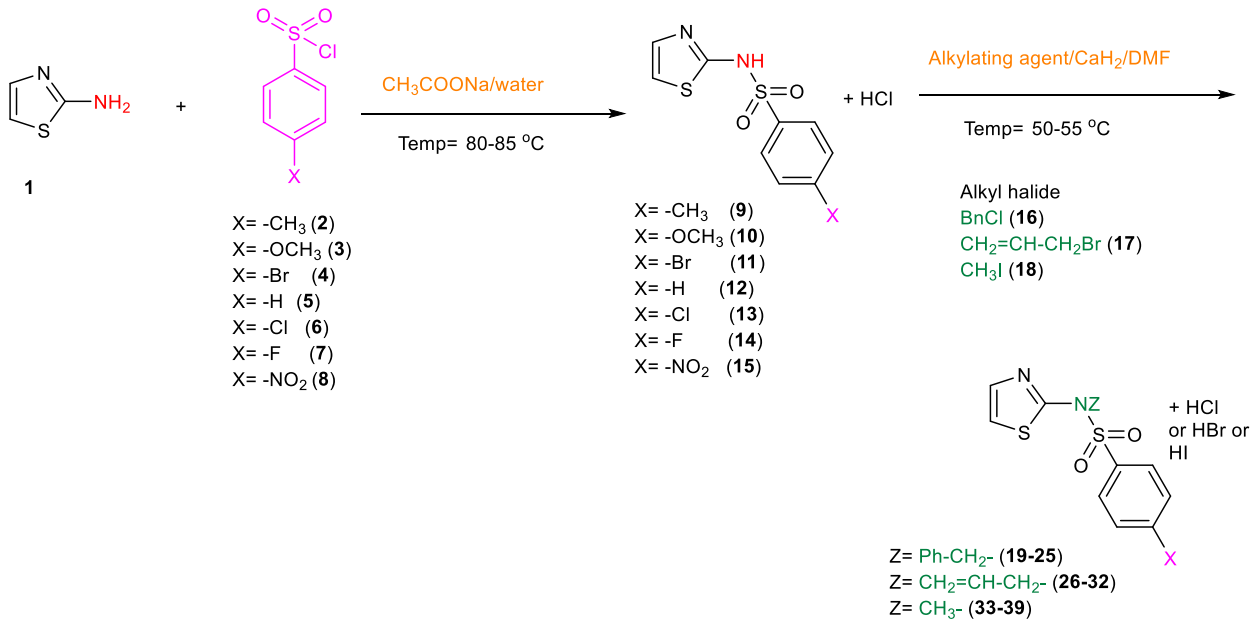

Scheme 1. N-sulfonylated N-alkylated aminothiazole synthesis (**19**–**39**).

increases their potency in the treatment of bacterial infections. Its versatility and reactivity in producing sulfonamide derivatives is probably the reason why 2-aminothiazole was chosen for the synthesis of sulfonamides. Because 2-aminothiazole reacts easily with sulfonyl chlorides to generate sulfonamides efficiently, it is a useful starting material. Its accessibility and somewhat easy synthesis also make it a handy precursor for producing a variety of sulfonamide compounds with potentially useful pharmacological characteristics. Our goal is to explore novel modifications, like ring formation and metal binding, to create unique compounds from 2-aminothiazoles. We aim to advance scientific understanding by developing innovative molecules with diverse biological effects.

2. Materials and methods

2.1. Chemical syntheses

2.1.1. Experimental methodology details

Without any purification, chemicals from Acros Organics, Fluka, Alfa Aesar, Sigma Aldrich, and Merck were used. We utilized distilled solvents. Thin layer chromatography was used to track the course of the reaction. A computerized device was used to record melting points (up to 300 °C). A t80 + UV–Vis spectrophotometer was utilized for nanometer spectroscopic examination. Agilent FTIR

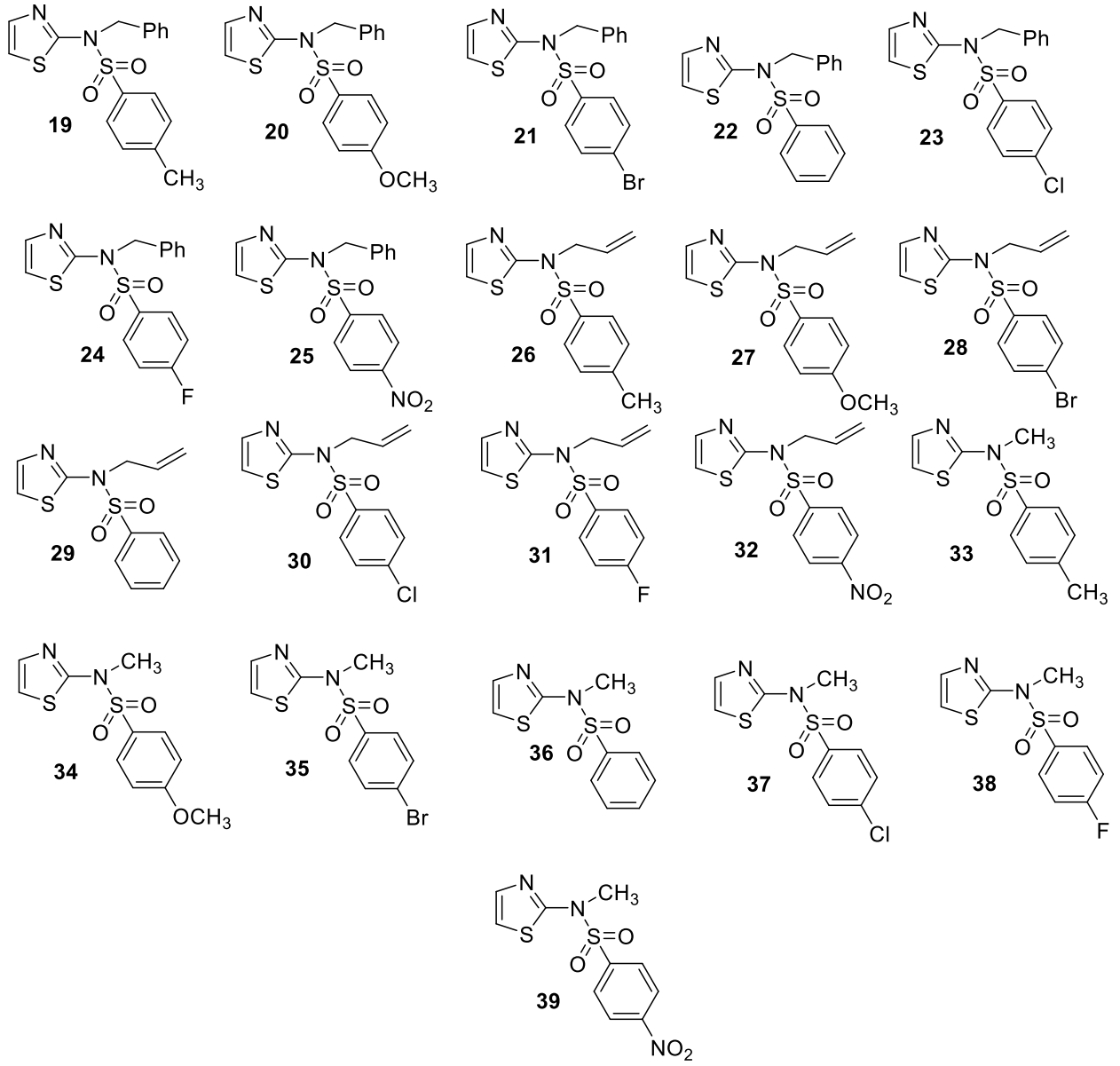

Scheme 2. Structure of compounds (19–39).

Cary 630 was used to obtain FTIR spectra (cm^{-1}). Using a Bruker NMR system, deuterated chloroform was utilized for NMR spectra; 300 MHz was employed for ^{1}H NMR and 75 MHz for ^{13}CNMR. Recorded are coupling constants in Hz and chemical changes in ppm.

2.1.2. General procedure for syntheses

2-Aminothiazole 1, a commercially available compound, served as the starting material for the synthesis of compounds. Following sulfonylation of the substrate, a series of N-sulfonylated intermediates (**9–15**) were obtained. These intermediates were subsequently subjected to alkylation reactions using alkylating agents (**16**–**18**), resulting in the formation of the desired alkylated compounds (**19**–**39**) in high yields. The complete synthetic procedure is illustrated in Schemes 1 and 2.

2.1.2.1. Procedure for N-sulfonylation of 2-aminothiazole (9–15). Sodium acetate was dissolved in water following a previously established protocol [37], after which sulfonyl chloride (**2**–**8**) and 2-aminothiazole 1 were introduced to the solution. The reaction mixture was heated to 80–85 °C and stirred continuously. Under these conditions, the initially yellow and sticky substance gradually transformed into a finely powdered solid. Upon completion of the reaction, as monitored by thin-layer chromatography (TLC) using a 2:1 ratio of n-hexane to ethyl acetate, the solid product was isolated by filtration. The product was then recrystallized from absolute ethanol to obtain pure compounds.

2.1.3. 4-Methyl-N-(thiazol-2-yl)benzenesulfonamide(9)

2-aminothiazole **1** (1 g, 0.00998 mol, 9.98 mmol), 4-methyl benzenesulfonyl chloride **2** (2.85 g, 14.97mmoles, 1.5 equiv.), distilled water (15 mL), sodium acetate (2.71 g, 19.96mmoles, 2 equiv.); **Temp:**80–85 °C; **Time:** 4 h; **Appearance:** light brown powder; **Yield:** 2.1 g (83 %); **R_f:**0.46; **M.P:** 150–152 °C;**M.W:** 254.289 g/mol; **Molecular Formula:**$C_{10}H_{10}N_2O_2S_2$; **FTIR**(cm^{-1})**:**3065 (sp^2 C–H Str.), 2923 (sp^3 C–H Str.), 1620 (w Ar C═C Bend.), 1588 (sp^2 C–N Bend.), 1496 (sp^3 C–H Bend.), 1350 (S═O Str.), 743 (Ar. C–H Bend.).

2.1.4. 4-Methoxy-N-(thiazol-2-yl)benzenesulfonamide(10)

2-aminothiazole**1** (1 g, 0.00998 mol, 9.98 mmol), 4-methoxy benzenesulfonyl chloride**3** (3.09 g, 14.97mmoles, 1.5 equiv.), distilled water (15 mL), sodium acetate (2.71 g, 19.96 mmol, 2 equiv.); **Temp:** 80-85 °C; **Time:**8 h; **Appearance:**dark brown powder; **Yield:** 2.2 g (82 %); **R_f:**0.54; **M.P:** 160-162 °C;**M.W:**270.289 g/mol; **Molecular Formula:**$C_{10}H_{10}N_2O_3S_2$; **FTIR**(cm^{-1})**:** 3062 (sp^2 C–H Str.), 2929 (sp^3 C–H Str.), 1618 (wAr C═C Bend.), 1540 (sp^2 C–N Bend.),1458 (sp^3 C–H Bend.), 1380 (S═O Str.), 767 (Ar C–H Bend.).

2.1.5. 4-Bromo-N-(thiazol-2-yl)benzenesulfonamide(11)

2-aminothiazole**1** (1 g, 0.00998 mol, 9.98 mmol), 4-bromo benzenesulfonyl chloride**4** (3.06 g, 11.976mmoles, 1.2 equiv.), distilled water (15 mL), sodium acetate (2.02 g, 14.97 mmol, 1.5 equiv.); **Temp:** 80-85 °C; **Time:** 8 h; **Appearance:** light brown powder; **Yield:**2.8 g (88 %); **R_f:** 0.57; **M.P:**185–187 °C;**M.W:** 319.159 g/mol; **Molecular Formula:**$C_9H_7BrN_2O_2S_2$; **FTIR**(cm^{-1})**:** 3099 (sp^2 C–H Str.), 2996 (sp^3 C–H Str.), 1624 (wAr C═C Bend.), 1577 (sp^2 C–N Bend.), 1529 (sp^3 C–H Bend.), 1380 (S═O Str.), 765 (Ar C–H Bend.).

2.1.5.1. N-(Thiazol-2-yl)benzenesulfonamide(12). 2-aminothiazole**1** (1 g, 0.00998 mol, 9.98 mmol), benzenesulfonyl chloride **5** (1.93 g, 10.978 mmoles, 1.1 equiv.), distilled water (15 mL), sodium acetate (2.03 g, 14.97mmoles, 1.5 equiv.); **Temp:** 80-85 °C; **Time:** 6 h; **Appearance:** dark brown powder; **Yield:** 1.92 g (80 %); **R_f:** 0.47; **M.P:** 140-142 °C;**M.W:** 240.259 g/mol; **Molecular Formula:** $C_9H_8N_2O_2S_2$;**FTIR**(cm^{-1})**:** . 3110 (sp^2 C–H Str.), 2953 (sp^3 C–H Str.), 1627 (wAr C═C Bend.), 1565 (sp^2 C–N Bend.), 1465 (sp^3 C–H Bend.), 1235 (S═O Str.), 736 (Ar C–H Bend.).

2.1.6. 4-Chloro-N-(thiazol-2-yl)benzenesulfonamide(13)

2-aminothiazole**1** (1 g, 0.00998 mol, 9.98 mmol), 4-chloro benzenesulfonyl chloride **6** (3.15 g, 14.97 mmol, 1.5 equiv.), distilled water (15 mL), sodium acetate (2.71 g, 19.96 mmol, 2 equiv.); **Temp:** 80-85 °C; **Time:** 8 h;**Appearance:**dark brown powder; **Yield:** 2.3 g (84 %); **R_f:**0.39; **M.P:** 162-164 °C;**M.W:**274.709 g/mol; **Molecular Formula:**$C_9H_7ClN_2O_2S_2$;**FTIR**(cm^{-1})**:** 3106 (sp^2 C–H Str.), 2951 (sp^3 C–H Str.), 1620 (wAr C═C Bend.), 1586 (sp^2 C–N Bend.), 1458 (sp^3 C–H Bend.), 1319 (S═O Str.), 758 (Ar C–H Bend.).

2.1.6.1. 4-Fluoro-N-(thiazol-2-yl)benzenesulfonamide(14). 2-aminothiazole**1** (1 g, 0.00998 mol, 9.98 mmol), 4-fluorobenzenesulfonyl chloride **7** (2.91 g, 14.97 mmol, 1.5 equiv.), distilled water (15 mL), sodium acetate (2.71 g, 19.96 mmol, 2 equiv.); **Temp:** 80-85 °C; **Time:** 8 h; **Appearance:** dark brown powder; **Yield:** 2.1 g (82 %); **R_f:** 0.29; **M.P:** 154-156 °C;**M.W:** 258.249 g/mol; **Molecular Formula:**$C_9H_7FN_2O_2S_2$;**FTIR**(cm^{-1})**:**3121 (sp^2 C–H Str.), 2954 (sp^3 C–H Str.), 1626 (wAr C═C Bend.), 1507 (sp^2 C–N Bend.), 1472 (sp^3 C–H Bend.), 1303 (S═O Str.), 706 (Ar C–H Bend.).

2.1.6.2. 4-Nitro-N-(thiazol-2-yl)benzenesulfonamide(15). 2-aminothiazole**1** (1 g, 0.00998 mol, 9.98 mmol), 4-nitro benzenesulfonyl chloride **8** (2.43 g, 10.978 mmol, 1.1 equiv.), distilled water (15 mL), sodium acetate (2.03 g, 14.97mmoles, 1.5 equiv.); **Temp:** 80-85 °C; **Time:** 4 h; **Appearance:** light brown powder; **Yield:**2 g (70 %); **R_f:** 0.32; **M.P:**168–170 °C;**M.W:** 285.259 g/mol; **Molecular Formula:**$C_9H_7N_3O_4S_2$; **FTIR**(cm^{-1}): 3070(sp^2 C–H Str.),2999 (sp^3 C–H Str.), 1623 (wAr C═C Bend.), 1522 (sp^2 C–N Bend.), 1457 (sp^3 C–H Bend.), 1380 (S═O Str.), 758 (Ar C–H Bend.).

2.1.6.3. Procedure for the syntheses of target compounds (19–39). N-sulfonamides were treated with calcium hydride in DMF at 50–55 °C with continuous stirring, following the protocol described [38]. After 30 min, the alkylating agents (**16**–**18**) were introduced

to the reaction mixture. Upon completion, as verified by thin-layer chromatography (TLC) using an n-hexane to ethyl acetate ratio of 8:2, the reaction mixture was cooled and diluted with cold distilled water before filtration. The absorption maxima (λ_{max}) of the products were determined using a 0.01 mmol solution in $CHCl_3$. The resulting crystalline products were further purified by recrystallization in absolute ethanol and by column chromatography, yielding the final compounds (**19**–**39**).

2.1.7. N-Benzyl-4-methyl-N-(thiazol-2-yl)benzenesulfonamide (19)

4-Methyl-*N*-(thiazol-2-yl)benzenesulfonamide**9** (1 g, 3.93mmoles), benzyl chloride **16** (0.99 g, 7.86 mmoles, 2 equiv.), DMF (5 mL), calcium hydride (0.496 g, 11.79mmoles, 3 equiv.); **Appearance:** light brown crystals; **Yield:** 1.1 g (81 %);**R_f:** 0.6; **M.P:** 190-192 °C;**M.W:** 344.369 g/mol; **Molecular Formula:**$C_{17}H_{16}N_2O_2S_2$**; UV/Vis:** (λ_{max}, 0.01 mmol, $CHCl_3$) 265 nm; **FTIR**(cm^{-1})**:**3063 (sp^2 C–H Str.), 2952 (sp^3 C–H Str.), 1618 (wAr C═C Bend.), 1553 (sp^2 C–N Bend.), 1453 (sp^3 C–H Bend.), 1358 (S═O Str.), 746 (Ar C–H Bend.); **^{1}H NMR:** δ 7.65 (d, 2H ^3J = 8.2 Hz) 7.41 (d, 2H ^3J = 8.2 Hz), 7.38–6.97(m,7H, aromatic region), 5.11 (s,2H, methylene of benzyl group), 2.42 (s, 3H, Methyl group); **^{13}C NMR:** δ 160.92 (N–C═N), 144.67 (C–N thiazole ring), 138.74, 135.81, 135.05, 129.84, 128.40, 128.38, 127.69, 127.42, 116.64, 53.16 (methylene carbon).

2.1.8. N-Benzyl-4-methoxy-N-(thiazol-2-yl)benzenesulfonamide (20)

4-Methoxy-*N*-(thiazol-2-yl)benzenesulfonamide**10** (1 g, 3.69mmoles), benzyl chloride **16** (0.934 g, 7.38mmoles, 2 equiv.), DMF (5 mL), calcium hydride (0.465 g, 11.07mmoles, 3 equiv.); **Appearance:** light brown crystals; **Yield:** 1.07 g (80 %); **R_f:** 0.4; **M.P:** 200-202 °C; **M.W:** 360.369 g/mol; **Molecular Formula:**$C_{17}H_{16}N_2O_3S_2$; **UV/Vis:** (λ_{max}, 0.01 mmol, $CHCl_3$) 264 nm; **FTIR**(cm^{-1})**:**3083 (sp^2 C–H Str.), 2929 (sp^3 C–H Str.), 1625 (wAr C═C Bend.), 1573 (sp^2 C–N Bend.), 1453 (sp^3 C–H Bend.), 1381 (S═O Str.), 776 (Ar C–H Bend.); **^{1}H NMR:** δ 7.79 (d, 2H ^3J = 8.6 Hz) 7.41 (d, 2H ^3J = 8.6 Hz), 7.39–6.90 (m,7H, aromatic region), 4.32 (s,2H, methylene of benzyl group), 3.90 (s, 3H, Methoxy group); **^{13}C NMR:** δ 162.77 (N–C═N), 135.74 (C–N, thiazole ring), 134.35, 132.35, 129.35, 128.97, 128.70, 128.58, 128.43, 127.64, 114.23, 55.67, 54.24 (methylene carbon).

2.1.8.1. N-benzyl-4-bromo-N-(thiazol-2-yl)benzenesulfonamide (21). 4-Bromo-*N*-(thiazol-2-yl)benzenesulfonamide**11** (1 g, 3.13mmoles), benzyl chloride **16** (0.79 g, 6.26 mmoles, 2 equiv.), DMF (5 mL), calcium hydride (0.395 g, 9.39mmoles, 3 equiv.); **Appearance:** light brown crystals; **Yield:** 1.02 g (80 %); **R_f:** 0.53; **M.P:** 232-234 °C;**M.W:** 414.85 g/mol; **Molecular Formula:** $C_{16}H_{13}BrN_2O_2S_2$; **UV/Vis:** (λ_{max}, 0.01 mmol, $CHCl_3$) 261 nm; **FTIR**(cm^{-1})**:**3064 (sp^2 C–H Str.), 2976 (sp^3 C–H Str.), 1618 (wAr C═C Bend.), 1573 (sp^2 C–N Bend.), 1450 (sp^3 C–H Bend.), 1338 (S═O Str.), 743 (Ar C–H Bend.); **^{1}H NMR:** δ 7.60 (d, 2H ^3J = 8.1Hz) 7.40(d, 2H ^3J = 8.1 Hz), 7.39–7.01 (m, 7H, aromatic region), 5.11 (s, 2H, methylene of benzyl group); **^{13}C NMR:** δ 160.58 (N–C═N), 138.99 (C–N, thiazole ring), 137.05, 135.33, 132.46, 128.90, 128.83, 128.53, 128.47, 127.91, 117.14, 53.61 (methylene carbon).

2.1.9. N-Benzyl-N-(thiazol-2-yl)benzenesulfonamide (22)

N-(Thiazol-2-yl)benzenesulfonamide**12**(1 g, 4.16 mmoles), benzyl chloride **16** (1.05 g, 8.32mmoles, 2 equiv.), DMF (5 mL), calcium hydride (0.525 g, 12.48mmoles, 3 equiv.); **Appearance:** light brown crystals; **Yield:** 1.1 g (80 %); **R_f:** 0.5; **M.P:** 178-180 °C;**M.W:** 330.339 g/mol; **Molecular Formula:**$C_{16}H_{14}N_2O_2S_2$;**UV/Vis:** (λ_{max}, 0.01 mmol, $CHCl_3$) 270 nm; **FTIR**(cm^{-1})**:**3063(sp^2 C–H Str.), 2963 (sp^3 C–H Str.), 1620 (wAr C═C Bend.), 1584 (sp^2 C–N Bend.), 1458 (sp^3 C–H Bend.), 1423 (S═O Str.), 753 (Ar C–H Bend.); **^{1}H NMR:** δ 7.78 (d, 2H^{3}J = 8.2Hz), 7.61 (d, 1H^{3}J = 7.2Hz), 7.46 (d, 2H^{3}J = 8.2Hz), 7.26–7.39 (m,5H), 6.99 (d, 1H^{3}J = 7.2Hz), 5.92 (m, 1H), 5.32 (dd, 1H), 5.19 (dd, 1H), 5.13 (s,2H); **^{13}C NMR:** δ 160.77, 138.78, 138.02, 135.65, 133.67, 129.24, 128.42, 127.77, 127.37, 116.77, 53.26.

2.1.9.1. N-benzyl-4-chloro-N-(thiazol-2-yl)benzenesulfonamide (23). 4-Chloro-*N*-(thiazol-2-yl)benzenesulfonamide**13**(1 g, 3.64 mmoles), benzyl chloride **16** (0.92 g, 7.28 mmoles, 2 equiv.), DMF (5 mL), calcium hydride (0.459g, 10.92 mmoles, 3 equiv.); **Appearance:** brown crystals; **Yield:** 1.07 g (81 %); **R_f:** 0.60; **M.P:** 198-200 °C;**M.W:** 364.789 g/mol; **Molecular Formula:** $C_{16}H_{13}ClN_2O_2S_2$;**UV/Vis:** (λ_{max}, 0.01 mmol, $CHCl_3$) 266 nm; **FTIR**(cm^{-1})**:**3083 (sp^2 C–H Str.), 2971 (sp^3 C–H Str.), 1624 (wAr C═C Bend.), 1584 (sp^2 C–N Bend.), 1466 (sp^3 C–H Bend.), 1371 (S═O Str.), 777 (Ar C–H Bend.); **^{1}H NMR:** δ 7.71 (d, 2H ^3J = 9.0Hz) 7.66(d, 2H ^3J = 9.0 Hz), 7.46–7.01(m,7H, aromatic region), 5.12 (s,2H, methylene of benzyl group); **^{13}C NMR:** δ 160.59(N–C═N), 140.25 (C–N, thiazole ring), 138.98, 136.51, 135.35, 129.48, 128.85, 128.53, 128.47, 127.90, 117.13, 53.59 (methylene carbon).

2.1.9.2. N-benzyl-4-fluoro-N-(thiazol-2-yl)benzenesulfonamide (24). 4-Fluoro-*N*-(thiazol-2-yl)benzenesulfonamide **14**(1 g, 3.87mmoles), benzyl chloride **16** (0.97 g, 7.74mmoles, 2 equiv.), DMF (5 mL), calcium hydride (0.488g, 11.6 mmoles, 3 equiv.); **Appearance:** light brown crystals; **Yield:** 1.07 g (80 %); **R_f:** 0.57; **M.P:** 192-194 °C;**M.W:** 348.329 g/mol; **Molecular Formula:** $C_{16}H_{13}FN_2O_2S_2$;**UV/Vis:** (λ_{max}, 0.01 mmol, $CHCl_3$) 263 nm; **FTIR**(cm^{-1})**:**3073(sp^2 C–H Str.), 2964 (sp^3 C–H Str.), 1624 (wAr C═C Bend.), 1584 (sp^2 C–N Bend.), 1453 (sp^3 C–H Bend.), 1344 (S═O Str.), 777 (Ar C–H Bend.); **^{1}H NMR:** δ 7.80 (d, 2H^{3}J = 9.1Hz), 7.76 (d, 2H^{3}J = 7.2Hz), 7.30 (d, 2H^{3}J = 8.2Hz), 7.16 (d,2H^{3}J = 7.2Hz), 5.12 (s,2H); **^{13}C NMR:** δ 167.32, 163.92, 160.70, 138.93, 135.41, 134.08, 130.31, 130.19, 128.50, 128.46, 127.88, 117.88, 116.65, 116.35, 53.52.

2.1.9.3. N-benzyl-4-nitro-N-(thiazol-2-yl)benzenesulfonamide (25). 4-Nitro-*N*-(thiazol-2-yl)benzenesulfonamide **15**(1 g, 3.50mmoles), benzyl chloride **16** (0.886 g, 7mmoles, 2 equiv.), DMF (5 mL), calcium hydride (0.441g, 10.5mmoles, 3 equiv.); **Appearance:** yellow brown crystals; **Yield:** 1.02 g (78 %); **R_f:** 0.36; **M.P:** 206-208 °C;**M.W:** 375.331 g/mol; **Molecular Formula:**$C_{16}H_{13}N_3O_4S_2$; **UV/Vis:** (λ_{max}, 0.01 mmol, $CHCl_3$) 261 nm; **FTIR**(cm^{-1})**:**3064 (sp^2 C–H Str.), 2923 (sp^3 C–H Str.), 1624 (wAr C═C Bend.), 1584 (sp^2 C–N

Bend.), 1478 (sp^3 C–H Bend.), 1368 (S═O Str.), 747(Ar C–H Bend.); **^{1}H NMR:** δ 8.31 (d, 2H ^3J = 9.2 Hz) 7.91(d, 2H ^3J = 9.2 Hz), 7.89–7.07 m,7H, aromatic region), 5.14 (s,2H, methylene of benzyl group); **^{13}C NMR:** δ 160.92 (N–C═N), 144.67 (C–N, thiazole ring), 138.74, 135.81, 135.05, 134.79, 128.79, 128.72, 128.20, 124.27, 117.86, 54.27 (methylene carbon).

2.1.10. N-Allyl-4-methyl-N-(thiazol-2-yl)benzenesulfonamide (26)

4-Methyl-*N*-(thiazol-2-yl)benzenesulfonamide**9** (1 g, 3.93mmoles), allyl bromide**17** (0.95 g, 7.86 mmoles, 2 equiv.), DMF (5 mL), calcium hydride (0.496 g, 11.79mmoles, 3 equiv.); **Appearance:**light brown crystals; **Yield:** 1 g (86 %); **R_f:** 0.42; **M.P:** 177-179 °C;**M.W:** 294.369 g/mol; **Molecular Formula:**$C_{13}H_{14}N_2O_2S_2$; **UV/Vis:** (λ_{max}, 0.01 mmol, $CHCl_3$) 271 nm; **FTIR**(cm^{-1})**:**3082 (sp^2 C–H Str.), 2950 (sp^3 C–H Str.), 1620 (wAr C═C Bend.), 1570 (sp^2 C–N Bend.), 1472 (sp^3 C–H Bend.), 1350 (S═O Str.), 743 (Ar C–H Bend.); **^{1}H NMR:** δ 7.70 (d, 2H ^3J = 9.2Hz), 7.41 (d, 1H ^3J = 9.8Hz),7.41 (d, 2H ^3J = 9.2Hz), 7.01 (d, 1H ^3J = 9.8Hz), 5.86 (m, 1H), 5.26 (m, 1H), 5.18 (m, 1H), 4.56 (d, 2H ^3J = 7.8Hz), 2.49 (s, 3H); **^{13}C NMR:** δ 161.13 (N═C═S), 151.45, 144.71, 138.71, 135.12, 129.81,127.51,118.78 (=CH_2), 116.15 (=CH), 52.24 (CH_2), 21.65 (CH_3)

2.1.10.1. N-allyl-4-methoxy-N-(thiazol-2-yl)benzenesulfonamide (27). 4-Methoxy-*N*-(thiazol-2-yl)benzenesulfonamide**10** (1 g, 3.69mmoles), allyl bromide**17**(0.892 g, 7.38mmoles, 2 equiv.), DMF (5 mL), calcium hydride (0.465 g, 11.07mmoles, 3 equiv.); **Appearance:** light brown crystals; **Yield:** 0.91 g (80 %); **R_f:** 0.32; **M.P:** 185-187 °C;**M.W:**310.369 g/mol; **Molecular Formula:** $C_{13}H_{14}N_2O_3S_2$; **UV/Vis:** (λ_{max}, 0.01 mmol, $CHCl_3$) 280 nm; **FTIR**(cm^{-1})**:**3062 (sp^2 C–H Str.), 2954 (sp^3 C–H Str.), 1622 (wAr C═C Bend.), 1570 (sp^2 C–N Bend.), 1478 (sp^3 C–H Bend.), 1363 (S═O Str.), 754 (Ar C–H Bend.); **^{1}H NMR:** δ 7.76 (d, 2H^{3}J = 8.2Hz), 7.41 (d, 1H^{3}J = 7.2Hz), 6.69 (d, 2H^{3}J = 8.2Hz), 6.69 (d, 1H^{3}J = 7.2Hz), 5.92 (m, 1H), 5.32 (dd, 1H), 5.19 (dd, 1H), 4.56 (s, 2H), 3.86 (m, 3H); **^{13}C NMR:** δ 163.68, 161.00, 138.69, 132.08, 129.75, 129.56, 118.74, 116.04, 114.34, 55.67, 52.20.

2.1.11. N-Allyl-4-bromo-N-(thiazol-2-yl)benzenesulfonamide (28)

4-Bromo-*N*-(thiazol-2-yl)benzenesulfonamide **11** (1 g, 3.13mmoles), allyl bromide**17**(0.75 g, 6.26 mmoles, 2 equiv.), DMF (5 mL), calcium hydride (0.395 g, 9.39mmoles, 3 equiv.); **Appearance:** light brown crystals; **Yield:** 0.95 g (84 %); **R_f:** 0.60; **M.P:** 210-212 °C; **M.W:**359.239 g/mol; **Molecular Formula:**$C_{12}H_{11}BrN_2O_2S_2$;**UV/Vis:** (λ_{max}, 0.01 mmol, $CHCl_3$) 267 nm; **FTIR**(cm^{-1})**:**3068 (sp^2 C–H Str.), 2996 (sp^3 C–H Str.), 1618 (wAr C═C Bend.), 1572 (sp^2 C–N Bend.), 1478 (sp^3 C–H Bend.), 1364 (S═O Str.), 764 (Ar C–H Bend.); **^{1}H NMR:** δ 7.64 (d, 2H ^3J = 8.1Hz), 7.43 (d, 1H ^3J = 8.1Hz), 7.14 (d, 2H ^3J = 8.3Hz), 7.05 (d, 1H ^3J = 8.3Hz), 5.87 (m, 1H), 5.32 (m, 1H), 5.17 (m, 1H), 4.56 (d, 2H ^3J = 7.8Hz); **^{13}C NMR:** δ 162.23 (N═C═S), 153.43, 139.00, 137.10, 132.48, 131.69,129.03,128.90,119.26(=CH_2), 116.70 (=CH), 52.56 (CH_2).

2.1.11.1. N-allyl-N-(thiazol-2-yl)benzenesulfonamide (29). *N*-(Thiazol-2-yl)benzenesulfonamide **12** (1 g, 4.16 mmoles), allyl bromide**17**(1 g, 8.32mmoles, 2 equiv.), DMF (5 mL), calcium hydride (0.525 g, 12.48mmoles, 3 equiv.); **Appearance:**dark brown crystals; **Yield:** 1 g (86 %); **R_f:** 0.53; **M.P:** 165-167 °C;**M.W:** 280.339 g/mol; **Molecular Formula:**$C_{12}H_{12}N_2O_2S_2$;**UV/Vis:** (λ_{max}, 0.01 mmol, $CHCl_3$) 270 nm; **FTIR**(cm^{-1})**:**3097 (sp^2 C–H Str.), 2953(sp^3 C–H Str.), 1627 (wAr C═C Bend.), 1563 (sp^2 C–N Bend.), 1478 (sp^3 C–H Bend.), 1369 (S═O Str.), 754 (Ar C–H Bend.); **^{1}H NMR:** δ 7.86–7.52 (M, 5H),7.28 (d, 1H ^3J = 8.1Hz), 7.02(d, 1H ^3J = 8.1Hz), 5.90 (m, 1H), 5.26 (m, 1H), 5.15 (m, 1H), 4.55 (d, 2H ^3J = 8.0Hz); **^{13}C NMR:** δ 160.77 (N═C═S), 138.77, 138.12, 133.69, 131.98, 131.92,129.21,127.47,118.89,118.86(=CH_2), 116.28 (=CH), 52.34 (CH_2).

2.1.12. N-Allyl-4-chloro-N-(thiazol-2-yl)benzenesulfonamide (30)

4-Chloro-*N*-(thiazol-2-yl)benzenesulfonamide **13**(1 g, 3.22mmoles), allyl bromide**17**(0.77 g, 6.44mmoles, 2 equiv.), DMF (5 mL), calcium hydride (0.406 g, 9.66 mmoles, 3 equiv.); **Appearance:** light brown crystals; **Yield:** 0.92 g (81 %); **R_f:** 0.60; **M.P:** 187-189 °C; **M.W:** 314.789 g/mol; **Molecular Formula:**$C_{12}H_{11}ClN_2O_2S_2$;**UV/Vis:** (λ_{max}, 0.01 mmol, $CHCl_3$) 277 nm; **FTIR**(cm^{-1})**:**3066(sp^2 C–H Str.), 2951(sp^3 C–H Str.), 1620 (wAr C═C Bend.), 1568 (sp^2 C–N Bend.), 1482(sp^3 C–H Bend.), 1364 (S═O Str.), 752 (Ar C–H Bend.);**^{1}H NMR:** δ 7.77 (d, 2H^{3}J = 9.1Hz), 7.46 (d, 2H^{3}J = 7.2Hz), 7.28 (d, 1H^{3}J = 8.2Hz), 7.02 (d,1H^{3}J = 7.2Hz), 6.94 (m, 1H^{3}J = 7.2Hz), 5.32 (m, 1H), 5.30 (dd, 1H), 5.54 (s,2H); **^{13}C NMR:** δ 160.51, 140.34, 138.99, 136.52, 131.75, 131.68, 129.52, 129.00, 119.27, 116.27, 52.64.

2.1.13. N-Allyl-4-fluoro-N-(thiazol-2-yl)benzenesulfonamide (31)

4-Fluoro-*N*-(thiazol-2-yl)benzenesulfonamide **14**(1 g, 3.87mmoles), allyl bromide**17**(0.93 g, 7.74mmoles, 2 equiv.), DMF (5 mL), calcium hydride (0.488 g, 11.61mmoles, 3 equiv.); **Appearance:** light brown crystals; **Yield:** 1 g (87 %); **R_f:** 0.52; **M.P:** 181-183 °C; **M.W:** 298.329 g/mol; **Molecular Formula:**$C_{12}H_{11}FN_2O_2S_2$;**UV/Vis:** (λ_{max}, 0.01 mmol, $CHCl_3$) 278 nm; **FTIR**(cm^{-1})**:**3072 (sp^2 C–H Str.), 2954 (sp^3 C–H Str.), 1626 (wAr C═C Bend.), 1567 (sp^2 C–N Bend.), 1463 (sp^3 C–H Bend.), 1363 (S═O Str.), 768 (Ar C–H Bend.); **^{1}H NMR:** δ 7.86 (d, 2H ^3J = 9.1Hz), 7.43 (d, 2H ^3J = 9.1Hz), 7.20 (d, 1H ^3J = 8.0Hz), 7.06 (d, 1H ^3J = 8.0Hz), 5.91 (m, 1H), 5.20 (m, 1H), 5.16 (m, 1H), 4.54 (d, 2H ^3J = 7.8Hz).; **^{13}C NMR:** δ 167.38 (N═C═S), 163.98, 160.62,138.98, 134.15, 131.1, 131.74, 130.45,120.32,119.17(=CH_2), 116.59 (=CH), 52.34 (CH_2).

2.1.13.1. N-Allyl-4-nitro-N-(thiazol-2-yl)benzenesulfonamide (32). 4-Nitro-*N*-(thiazol-2-yl)benzenesulfonamide **15** (1 g, 3.50mmoles), allyl bromide **17** (0.84 g, 7mmoles, 2 equiv.), DMF (5 mL), calcium hydride (0.442 g, 10.5mmoles, 3 equiv.); **Appearance:** brown crystals; **Yield:** 0.9 g (79 %); **R_f:** 0.42; **M.P:** 193-195 °C; **M.W:**325.339 g/mol; **Molecular Formula:**$C_{12}H_{11}N_3O_4S_2$; **UV/Vis:** (λ_{max}, 0.01 mmol, $CHCl_3$) 259 nm; **FTIR**(cm^{-1})**:**3066 (sp^2 C–H Str.), 2950 (sp^3 C–H Str.), 1623 (wAr C═C Bend.), 1561 (sp^2 C–N Bend.), 1485

(sp^3 C–H Bend.), 1362 (S═O Str.), 773 (Ar C–H Bend.); **^{1}H NMR:** δ 7.86 (d, 2H ^3J = 8.1Hz), 7.47 (d, 2H ^3J = 8.1Hz), 7.28 (d, 1H ^3J = 8.0Hz), 7.11 (d, 1H ^3J = 8.0Hz), 5.86 (m, 1H), 5.33 (m, 1H), 5.19 (m, 1H), 4.55 (d, 2H ^3J = 8.1Hz); **^{13}C NMR:** δ 160.05 (N═C═S), 150.53, 143.77, 139.34, 131.26, 128.99, 124.36, 119.88, 117.49(=CH_2), 116.15(=CH), 52.24 (CH_2).

2.1.13.2. N,4-Dimethyl-N-(thiazol-2-yl)benzenesulfonamide (33). 4-Methyl-*N*-(thiazol-2-yl)benzenesulfonamide**9** (1 g, 3.93mmoles), methyl iodide**18** (1.11 g, 7.86 mmoles, 2 equiv.), DMF (5 mL), calcium hydride (0.496 g, 11.79mmoles, 3 equiv.); **Appearance:** dark brown crystals; **Yield:** 0.9 g (86 %); **R_f:** 0.6; **M.P:** 167-169 °C;**M.W:** 268.318 g/mol; **Molecular Formula:**$C_{11}H_{12}N_2O_2S_2$; **UV/Vis:** (λ_{max}, 0.01 mmol, $CHCl_3$) 269 nm; **FTIR**(cm^{-1})**:**3063 (sp^2 C–H Str.), 2950 (sp^3 C–H Str.), 1616 (wAr C═C Bend.), 1554 (sp^2 C–N Bend.), 1443 (sp^3 C–H Bend.), 1364 (S═O Str.), 740 (Ar C–H Bend.); **^{1}H NMR:** δ 7.70 (d, 2H ^3J = 8.5Hz), 7.36(d, 2H ^3J = 8.5Hz),7.30 (d, 1H ^3J = 8.2Hz, thiazole ring), 6.69 (d, 1H ^3J = 8.2Hz, thiazole ring),3.42 (s, 3H, Methyl), 3.41 (s, 3H, Ar-Methyl);**^{13}C NMR:** δ 161.93 (N═C═N), 144.90, 138.40, 133.65, 129.92, 127.32, 115.68 (C–S), 36.52 (N–CH_3), 21.63 (Ar-CH_3).

2.1.14. 4-Methoxy-N-methyl-N-(thiazol-2-yl)benzenesulfonamide (34)

4-Methoxy-*N*-(thiazol-2-yl)benzenesulfonamide**10** (1 g, 3.69mmoles), methyl iodide**18**(1.04 g, 7.38mmoles, 2 equiv.), DMF (5 mL), calcium hydride (0.465 g, 11.07mmoles, 3 equiv.); **Appearance:** light brown crystals; **Yield:** 0.89 g (85 %); **R_f:** 0.28; **M.P:** 175-177 °C;**M.W:** 284.318 g/mol; **Molecular Formula:**$C_{11}H_{12}N_2O_3S_2$;**UV/Vis:** (λ_{max}, 0.01 mmol, $CHCl_3$) 288 nm; **FTIR**(cm^{-1})**:**2996 (sp^2 C–H Str.), 2943 (sp^3 C–H Str.), 1620 (wAr C═C Bend.), 1525 (sp^2 C–N Bend.), 1438 (sp^3 C–H Bend.), 1363 (S═O Str.), 752 (Ar C–H Bend.); **^{1}H NMR:** δ 7.77 (d, 2H ^3J = 8.5Hz), 7.73 (d, 2H ^3J = 8.5Hz),7.38 (d, 1H ^3J = 8.2Hz, thiazole ring), 6.94 (d, 1H ^3J = 8.2Hz, thiazole ring), 3.86 (s, 3H, O-Methyl), 3.42 (s, 3H, Methyl);**^{13}C NMR:** δ 163.82 (N═C═N), 138.39, 129.89, 129.52, 128.16, 115.60, 114.47 (C–S), 114.16, 55.67 (O–CH_3), 36.47 (N–CH_3).

2.1.15. 4-Bromo-N-methyl-N-(thiazol-2-yl)benzenesulfonamide (35)

4-Bromo-*N*-(thiazol-2-yl)benzenesulfonamide **11** (1 g, 3.13mmoles), methyl iodide**18**(0.88 g, 6.26 mmoles, 2 equiv.), DMF (5 mL), calcium hydride (0.395 g, 9.39mmoles, 3 equiv.); **Appearance:** light brown crystals; **Yield:** 0.88 g (85 %); **R_f:** 0.50; **M.P:** 210-212 °C; **M.W:**333.188 g/mol; **Molecular Formula:**$C_{10}H_9BrN_2O_2S_2$;**UV/Vis:** (λ_{max}, 0.01 mmol, $CHCl_3$) 269 nm; **FTIR**(cm^{-1})**:**3072 (sp^2 C–H Str.), 2924 (sp^3 C–H Str.), 1620 (wAr C═C Bend.), 1559 (sp^2 C–N Bend.), 1453 (sp^3 C–H Bend.), 1320 (S═O Str.), 753 (Ar C–H Bend.); **^{1}H NMR:** δ 7.69 (d, 2H ^3J = 8.5Hz), 7.67(d, 2H ^3J = 8.5Hz),7.40 (d, 1H ^3J = 8.2Hz, thiazole ring),7.02 (d, 1H ^3J = 8.2Hz, thiazole ring),3.43 (s, 3H, Methyl);**^{13}C NMR:** δ 161.49 (N═C═N), 138.68, 135.56, 132.64, 129.12, 128.77, 116.13 (C–S), 36.76 (N–CH_3).

2.1.16. N-Methyl-N-(thiazol-2-yl)benzenesulfonamide (36)

N-(Thiazol-2-yl)benzenesulfonamide **12** (1 g, 4.16 mmoles), methyl iodide**18**(1.18 g, 8.32mmoles, 2 equiv.), DMF (5 mL), calcium hydride (0.525 g, 12.48mmoles, 3 equiv.); **Appearance:** white crystals; **Yield:** 0.92 g (88 %); **R_f:** 0.41; **M.P:** 155-157 °C;**M.W:** 254.288 g/mol; **Molecular Formula:**$C_{10}H_{10}N_2O_2S_2$;**UV/Vis:** (λ_{max}, 0.01 mmol, $CHCl_3$) 279 nm; **FTIR**(cm^{-1})**:**3059 (sp^2 C–H Str.), 2953 (sp^3 C–H Str.), 1620 (wAr C═C Bend.), 1525 (sp^2 C–N Bend.), 1438 (sp^3 C–H Bend.), 1353 (S═O Str.), 746 (Ar C–H Bend.); **^{1}H NMR:** δ 7.83–7.60 (m, 5H), 7.39 (d, 1H ^3J = 8.2Hz, thiazole ring), 7.01 (d, 1H ^3J = 8.2Hz, thiazole ring),3.44 (s, 3H, Methyl);**^{13}C NMR:** δ 161.79 (N═C═N), 138.45, 136.65, 133.84, 129.32, 127.29, 115.79 (C–S), 36.60 (N–CH_3).

2.1.17. 4-Chloro-N-methyl-N-(thiazol-2-yl)benzenesulfonamide (37)

4-Chloro-*N*-(thiazol-2-yl)benzenesulfonamide **13** (1 g, 3.22mmoles), methyl iodide**18**(0.91 g, 6.44mmoles, 2 equiv.), DMF (5 mL), calcium hydride (0.406 g, 9.66 mmoles, 3 equiv.); **Appearance:** dark brown crystals; **Yield:** 0.88 g (84 %); **R_f:** 0.52; **M.P:** 177-179 °C; **M.W:** 288.738 g/mol; **Molecular Formula:**$C_{10}H_9ClN_2O_2S_2$;**UV/Vis:** (λ_{max}, 0.01 mmol, $CHCl_3$) 271 nm; **FTIR**(cm^{-1})**:**3063 (sp^2 C–H Str.), 2958 (sp^3 C–H Str.), 1620 (wAr C═C Bend.), 1525 (sp^2 C–N Bend.), 1443 (sp^3 C–H Bend.), 1363 (S═O Str.), 746 (Ar C–H Bend.); **^{1}H NMR:** δ 7.63 (d, 2H ^3J = 8.0Hz), 7.73 (d, 2H ^3J = 8.5Hz), 7.40 (d, 1H ^3J = 8.2Hz, thiazole ring), 7.02 (d, 1H ^3J = 8.2Hz, thiazole ring), 3.44 (s, 3H, Methyl);**^{13}C NMR:** δ 161.79 (N═C═N), 138.45, 135.65, 133.84, 129.32, 127.29, 115.79 (C–S), 36.60 (N–CH_3).

2.1.18. 4-Fluoro-N-methyl-N-(thiazol-2-yl)benzenesulfonamide (38)

4-Fluoro-*N*-(thiazol-2-yl)benzenesulfonamide **14** (1 g, 3.87mmoles), methyl iodide**18**(1.09 g, 7.74 mmol, 2 equiv.), DMF (5 mL), calcium hydride (0.488 g, 11.61mmoles, 3 equiv.); **Appearance:** light brown crystals; **Yield:** 0.89 g (85 %); **R_f:** 0.29; **M.P:** 169-171 °C; **M.W:** 272.278 g/mol; **Molecular Formula:**$C_{10}H_9FN_2O_2S_2$;**UV/Vis:** (λ_{max}, 0.01 mmol, $CHCl_3$) 278 nm; **FTIR**(cm^{-1})**:**3067 (sp^2 C–H Str.), 2959 (sp^3 C–H Str.), 1615 (wAr C═C Bend.), 1565 (sp^2 C–N Bend.), 1485 (sp^3 C–H Bend.), 1365 (S═O Str.), 765 (Ar C–H Bend.); **^{1}H NMR:** δ 7.85(d, 2H ^3J = 8.0Hz), 7.82(d, 2H ^3J = 8.5Hz),7.39 (d, 1H ^3J = 8.2Hz, thiazole ring), 7.03 (d, 1H ^3J = 8.2Hz, thiazole ring), 3.44 (s, 3H, Methyl); **^{13}C NMR:** δ 161.51 (N═C═N), 164.11, 161.62, 138.62, 132.68, 132.64, 130.20, 130.07, 116.82, 116.52, 116.04 (C–S), 36.70 (N–CH_3).

2.1.19. N-Methyl-4-nitro-N-(thiazol-2-yl)benzenesulfonamide (39)

4-Nitro-*N*-(thiazol-2-yl)benzenesulfonamide **15** (1 g, 3.50mmoles), methyl iodide**18** (0.99 g, 7mmoles, 2 equiv.), DMF (5 mL), calcium hydride (0.442 g, 10.5mmoles, 3 equiv.); **Appearance:**lightyellow crystals; **Yield:** 0.8 g (77 %); **R_f:** 0.59; **M.P:** 183-185 °C;**M.W:** 299.288 g/mol; **Molecular Formula:** $C_{10}H_9N_3O_4S_2$;**UV/Vis:** (λ_{max}, 0.01 mmol, $CHCl_3$) 259 nm; **FTIR**(cm^{-1})**:**3115 (sp^2 C–H Str.), 2955 (sp^3 C–H St), 1631 (wAr C═C Bend.), 1525 (sp^2 C–N Bend.), 1438 (sp^3 C–H Bend.), 1370 (S═O Str.), 772 (Ar C–H Bend.); **^{1}H NMR:** δ 8.38 (d, 2H ^3J = 8.2Hz), 7.99 (d, 2H ^3J = 8.2Hz),7.43 (d, 1H ^3J = 8.5Hz, thiazole ring),7.07 (d, 1H ^3J = 8.5Hz, thiazole

ring),3.48 (s, 3H, Methyl); **^{13}C NMR:** δ 160.99 (N═C═N), 150.69,142.16, 139.01, 128.70, 124.53,116.76 (C–S), 37.14 (N–CH_3).

2.2. Crystallographic techniques using X-rays and data collection

Compounds **19**, **23**, and **24** underwent powder X-ray diffraction at a Thermo Fisher Scientific powder X-ray diffractometer in the United States.

2.3. Urease inhibition assay

Ten minutes at 37 °C were used to pre-incubate 0.015 units of jack bean urease (Sigma) in an 85 μL assay mixture. After adding 40 μL of 20 mM urea substrate to each well, the Synergy HT plate reader was used to pre-read the results at 625 nm. To develop the color at 625 nm, 70 μL of alkali reagent and 45 μL of phenol were applied.

Inhibition (%) = 100-[(Abs. of sample/Abs. of control) × 100]

IC_{50} values were calculated using the EZ-Fit Enzyme program with percent inhibition data from serial dilutions of active substances tested (Perrella Inc., USA) [39].

2.4. α-Glucosidase and α-amylase inhibition assay

A solution of 0.1 g potato starch and 100 mL of 0.1 % w/v sodium acetate buffer was used to assess the activity of α-amylase. For the enzyme solution, 27.5 mg of α-amylase was dissolved in 100 mL of distilled water. Using 96 mM 3,5 di-nitro salicylic acid and sodium potassium tartrate, a colorimetric reagent was produced. Compounds and plant extract were mixed with a starch solution. The resulting 3-amino-5-nitro salicylic acid was used to calculate the amount of maltose generated after adding α-amylase and incubation at 25 °C. A UV/visible spectrophotometer (BMS, USA) was used to measure the absorbance at 540 nm in order to calculate the percentage of inhibition.

A 0.2 M Tris buffer (pH 8.0) and a 2 % w/v starch (sucrose) solution were used to test for alpha glucosidase inhibition. Following a 5-min incubation period at 37 °C, plant extracts and compounds (200–800 μg/mL) were combined with the starch solution and Tris buffer. Intermittent additions of 5 mM P-nitrophenyl-α-D glucopyranoside were made. Once added, α-Glucosidase (1 U/mL) was incubated at 35 °C for 40 min. A BMS spectrophotometer (USA) was used to detect the color intensity at 405 nm after the reaction was stopped with 6 N HCl [40].

% Inhibition = Abs Control−Abs Sample/Abs Control × 100

2.5. Antioxidant assay

2.5.1. DPPH free radical scavenging activity

The protocol was followed for the DPPH free radical scavenging experiment [41,42]. For 1 h, a reaction mixture containing 100 μL test samples (concentrations: 100, 250, 500, and 1000 μg) and 900 μL DPPH was incubated at 37 °C in the dark. Using ascorbic acid as the positive control and 3 % methanol as the blank, the spectrophotometric absorbance was measured at 517 nm.

Inhibition (%) = 100-(Absorbance of test sample/Absorbance of control) × 100.

2.5.2. ABTS method

Using ultrapure water, the antioxidant Assay Kit (Cat. no. CS0790) was used in duplicate assays. The ABTS substrate, the Trolox standard, and a viable solution were prepared. A trolox standard curve was created using 20 μL of myoglobin and 10 μL of trolox. There were two types of test samples: 10 μL and 20 μL myoglobin. After adding the ABTS substrate, the absorbance at 405 nm was measured [43].

2.5.3. Superoxide anion scavenging assay

The Nitro Blue Tetrazolium (NBT) technique was used to detect superoxide production [44]. Ascorbic acid, NBT, and NADH solutions with fractions were incorporated in the reaction mixture. The reaction was started by adding PMS solution, and the percentage inhibition was determined by comparing the optical density at 530 nm before and after illumination.

2.6. Medicinal chemistry, docking and MD simulation protocols

The chemical structures of the synthesized derivatives were drawn using ChemDraw® Ultra 12.February 0, 1076, and Chem3D Pro 12.February 0, 1076 was used to optimize them.The ADMETlab 2.0 server [45] and SwissADME [46] were used to estimate a number of the physiochemical properties, medicinal chemistry, absorption, distribution, metabolism, validation of toxicophoric rules, and toxicity indicators. The drug likeness, bioavailability score, passive absorption in the gastrointestinal tract, and permeability across the blood-brain barrier of the target motifs using the BOILED-Egg model were all measured using the SwissADME server. Furthermore, the

AutoDockTools-1.5.6 program was utilized to determine the ligand efficacies of tiny compounds against the target substrates and ligand-protein binding complexes with the lowest binding capabilities [47]. The produced compounds underwent molecular docking studies to assess the ligand interactions with different enzyme substrates. The evolutionary algorithm of the docking program was used to carry out the dockage simulations. The three-dimensional characteristics of the grid box were adjusted taking into account the appropriate spacing values for every distinct substrate. The genetic algorithm parameters were maintained at their default settings, with the exception of increasing the number of GA runs to 100 in order to increase the sampling. The substrate and ligands were selected during the docking setup. Further analysis and visualization were performed on the top docked energy complexes using the BIOVIA Discovery Studio software [48]. A precompiled binary application called NAMD 2.14 software [49] was utilized for molecular dynamics (MD) simulation studies of ligand-substrate complexes. Subsequently, VMD 1.9.3 [50] was utilized for the simulation setup, trajectory analysis, visualization, and additional investigations of simulated ligand-substrate complexes. The CHARMM general force field (CGenFF) [51,52] and a ligand reader and modeller based on the CHARMM graphical user interface [53,54] were used to construct ligand topologies.

3. Results and discussions

3.1. Target compounds

The synthesis, chemical studies, and biological activity of twenty one 2-aminothiazole derivatives were carried out. The compounds **20**, **21**, **23**, **25**, **27**, **28**, **30**, **31** and **32** are novel among the synthesized ones. Two steps were involved in designing the synthetic pathway: First, the amino group of 2-aminothiazole was sulfonylated; this was followed by the same group being N-alkylated. Furthermore, spectro-analytical methods were used to examine all chemicals (**19**–**39**). The compounds' UV spectra revealed absorption in the 259–288 nm range.

3.1.1. Chemistry

The chemical aspects of the methodology for N-sulfonylation of 2-aminothiazole involve nucleophilic substitution reactions between the amino group of 2-aminothiazole and sulfonyl chloride, facilitated by a base such as sodium acetate. Heating and stirring promote reaction kinetics and uniformity. Formation of a yellow sticky mass followed by powdered solid indicates intermediate and product formation. TLC monitoring allows tracking of reaction progress, while recrystallization purifies the product for subsequent characterization using techniques like NMR and IR spectroscopy. The alkylation process starts with the reductive alkylation of N-sulfonamides at 50–55 °C using calcium hydride in DMF. Next, an alkylating agent is added. The progress of the reaction is monitored using Thin Layer Chromatography (TLC), which uses an 8:2 ratio of n-hexane to ethyl acetate to guide the next steps. Upon confirmation of completion, the mixture is cooled, filtered post-addition of cold distilled water, likely precipitating out impurities. Spectroscopic analysis involves determining λ_{max} values using a $CHCl_3$ solution. Crystals obtained undergo further purification via column chromatography, separating product from impurities. Final refinement occurs through recrystallization in pure ethanol, yielding a purer product. This methodology amalgamates reductive chemistry, chromatographic purification, and spectroscopic analysis for effective synthesis and purification of the desired product from N-sulfonamides.

Based on the NMR data, it can be inferred that the compounds with benzyl group contain an aromatic ring and a methylene group. The presence of aromatic protons and carbons suggests a compound with an aromatic moiety. The compounds with allyl group contain an aromatic ring, and an olefinic bond. The presence of both aromatic and olefinic protons and carbons suggests a conjugated system. The compounds with methyl group contain a thiazole derivative with an aromaticringand carbons as well as a methyl group attached to a nitrogen atom.

The IR data of the final products shows that the compounds contain aromatic ring(ArC═C Bend. 1615 cm^{-1}-1631 cm^{-1}; ArC-H Bend. 740 cm^{-1}-777 cm^{-1}) and substituents like amino groups (C–N Bend. 1525 cm^{-1}-1584 cm^{-1}) and sulfur containing functional groups (S═O Str. 1344 cm^{-1}-1371 cm^{-1}).

The UV data indicates the presence of compounds with conjugated pi-electron systems, which are likely aromatic or contain multiple double bonds.

3.2. The packing of molecules in crystals of compounds 19, 23, and 24

The structural information and properties of **19** and **23** were investigated by using X-ray spectrometer. In the obtained XRD pattern of **19** and **23**, diffraction peaks at 12.90°, 16.40°, 18.05°, 19.35°, 31.19°, 22.11°, 38.32°,38.32°44.50°, 65.10°,78.41° have corresponding diffraction planes (020), (101), (101), (111), (121), (231), (121), (311),(123),(115),(420) respectively. XRD pattern of **19** and **23** (Fig. S43 supporting file) exposes our sample showing orthorhombic crystal system. These XRD results were matched according to literature (JCPDS No. = 00-030-1945). XRD was performed on the prepared sample **24**. The diffraction peaks for the compound 24 were seen at 24.07°, 26.51°, 34.54°, 41.95°, 44.51°, 56.07° have their respective diffraction planes (011), (140), (141),(241) (JCPDS No. = 00-032-1683). XRD pattern of **24** (Fig. S44 supporting file) exposes our sample showing monoclinic crystal system.

3.3. In vitro Urease inhibition assay

Samples with >50 % enzyme inhibition were IC_{50} assayed. Compounds **36**, **22**, **34**, and **35** demonstrated strong inhibition against Jack bean urease (J.B. urease) and *Bacillus Pasteurii* urease with IC_{50} values of 14.06 ± 0.03 μM/mL, 15.31 ± 0.09 μM/mL, 16.01 ±

0.21 μM/mL, and 18.71 ± 0.15 μM/mL for J.B. urease, and 17.06 ± 0.03 μM/mL, 18.03 ± 0.23 μM/mL, 18.70 ± 0.04 μM/mL, and 20.21 ± 0.19 μM/mLfor B.P urease respectively, compared to thiourea. Other compounds exhibited varied IC_{50} values, with **32** and **25** showing weak inhibition against both enzymes (Table 1). Urease affects urinary and digestive tracts, contributing to conditions like urolithiasis, pyelonephritis, and gastritis. Inhibitors can help manage urease activity, essential for treatment and cultivation [55].

Soil enzymes, bacteria, fungus, and higher plants all include ureases [56]. Urinary stone formation, peptic ulcers, hepatic coma, and pyelonephritis are among the ailments that are attributed to bacterial ureases [57]. Urease activity, by releasing excess ammonia after urea fertilization, poses ecological and economic challenges in agriculture, leading to plant damage and soil pH elevation. Recent developments include urease inhibitors like fluorofamide, hydroxyureas, and hydroxamic acids, gaining attention as potential anti-ulcer drugs [58].

3.4. In vitro α-glucosidase and α-amylase inhibition assay

Samples with >50 % enzyme inhibition were assayed for IC_{50}. Compounds **20**, **26**, **21**, **29**, **30**, **31**, and **32** exhibited potent inhibitory effects against α-glucosidase and α-amylase, with IC_{50} values ranging from 20.34 μM/mL to 32.01 μM/mL for α-glucosidase and 25.09 μM/mLto 37.20 μM/mLfor α-amylase, compared to the standard Glimepiride (IC_{50} = 18.02 μM/mL for α-glucosidase, IC_{50} = 23.02 μM/Ml for α-amylase). Other compounds showed mild to moderate enzyme inhibition, while **39**, **24**, **37**, **36**, **35**, **34**, and **33** showed weak inhibition against both enzymes (Table 2). Postprandial Hyperglycemia, a precursor to diabetes, is linked to α-glucosidase and α-amylase, making their inhibition a potential strategy for managing hyperglycemia. Phenolic compounds like phenols, terpenoids, and flavonoids are natural α-glucosidase inhibitors, aiding glucose regulation. In diabetes, oxidative damage occurs due to reactive oxygen free radicals, emphasizing the importance of insulin in glucose regulation. Inhibiting α-amylase and α-glucosidase helps reduce glucose absorption and manage blood glucose levels, presenting a promising avenue for diabetes management [59–64].

3.5. In vitro DPPH free radical scavenging, ABTS, and superoxide scavenging activity

The compounds demonstrated strong antioxidant effects. Specifically, compounds **33**, **26**, and **27** exhibited potent scavenging against DPPH, with IC_{50} values of approximately 34.4, 38.3, and 39.2 μM/mL respectively. In addition, compounds **26** and **33** showed excellent efficacy against ABTS, with IC_{50} values of about 33.01 and 35.09 μM/mL respectively. Compound **26** was also effective in scavenging superoxide anion radicals, with an IC_{50} value of approximately 36 μM/mL. Other compounds had varying levels of scavenging effects against these radicals, ranging from moderate to weak (Table 3).

Compounds **21**, **28**, and **36** demonstrated strong scavenging against DPPH, with IC_{50} values of approximately 45.2 μM/mL, 48.4 μM/mL, and 49.3 μM/mL respectively. These same compounds were highly effective against ABTS, with IC_{50} values of about 33.01 μM/mL, 35.01 μM/mL, and 38.01 μM/mL respectively, as shown in Table 4. Additionally, compounds **35** and **28** showed effectiveness in scavenging superoxide anion radicals, with IC_{50} values of approximately 38 μM/mL and 39 μM/mL respectively. Other compounds displayed varying degrees of scavenging effects, ranging from moderate to weak (Table 4).

Table 1
Urease inhibition activities of compounds (**19**–**39**).

S.no	Compounds	Enzyme (SEM ±) μM/mL		Types of inhibition
		1. J.B Urease	B.P Urease	
2.	**19**	26.15 ± 0.02	29.05 ± 0.01	**Competitive**
3.	**26F**	30.11 ± 0.07	38.20 ± 0.36	**Non-competitive**
4.	**33**	22.05 ± 0.29	25.09 ± 0.14	**Non-competitive**
5.	**20**	20.55 ± 0.41	22.11 ± 0.35	**Competitive**
6.	**27**	24.13 ± 0.34	26.37 ± 0.22	**Competitive**
7.	**34**	16.01 ± 0.21	18.71 ± 0.15	**Competitive**
8.	**21**	23.06 ± 0.11	27.04 ± 0.48	**Non-competitive**
9.	**28**	29.55 ± 0.12	36.13 ± 0.43	**Non-competitive**
10.	**35**	18.70 ± 0.04	20.21 ± 0.19	**Competitive**
11.	**22**	15.31 ± 0.09	18.70 ± 0.23	**Competitive**
12.	**29**	21.22 ± 0.17	23.02 ± 0.15	**Non-competitive**
13.	**36**	14.06 ± 0.03	17.06 ± 0.03	**Competitive**
14.	**23**	25.10 ± 0.28	28.02 ± 0.07	**Non-competitive**
15.	**30**	28.09 ± 0.35	32.33 ± 0.37	**Non-competitive**
16.	**37**	21.02 ± 0.21	25.35 ± 0.31	**Competitive**
17.	**24**	32.11 ± 0.13	40.88 ± 0.26	**Competitive**
18.	**31**	46.02 ± 0.05	51.39 ± 0.11	**Non-competitive**
19.	**38**	24.31 ± 0.18	27.15 ± 0.14	**Competitive**
20.	**25**	48.11 ± 1.19	53.32 ± 0.21	**Non-competitive**
21.	**32**	52.05 ± 1.12	57.89 ± 0.18	**Non-competitive**
22.	**39**	38.17 ± 0.01	43.71 ± 0.13	**Non-competitive**
22.	Thiourea	10.12 ± 0.08	14.08 ± 0.05	–

Experiments = 3, Values = mean ± SEM.

Table 2
The α-Glucosidase and α-Amylase Inhibitory Activities of compounds (**19**–**39**).

Sr. No.	Compounds	Enzyme (% Inhibition ± SEM)μM/mL		Type of Inhibition
		23. α-Glucosidase± SEM	α-Amylase± SEM	
1.	**19**	32.13 ± 0.08	37.05 ± 0.11	**Competitive**
2.	**26**	22.18 ± 0.03	28.02 ± 0.27	**Competitive**
3.	**33**	69.09 ± 0.16	77.22 ± 0.12	**Competitive**
4.	**20**	20.34 ± 0.71	25.09 ± 0.23	**Non-competitive**
5.	**27**	34.22 ± 0.15	38.25 ± 0.11	**Non-competitive**
6.	**34**	63.03 ± 0.19	65.33 ± 0.13	**Non-competitive**
7.	**21**	25.07 ± 0.08	30.02 ± 0.27	**Competitive**
8.	**28**	37.12 ± 0.11	39.04 ± 0.10	**Competitive**
9.	**35**	60.60 ± 0.03	63.11 ± 0.16	**Competitive**
10.	**22**	39.41 ± 0.05	41.60 ± 0.12	**Non-competitive**
11.	**29**	27.12 ± 0.16	32.03 ± 0.14	**Non-competitive**
12.	**36**	59.05 ± 0.07	62.11 ± 0.12	**Non-competitive**
13.	**23**	41.14 ± 0.18	43.04 ± 0.05	**Non-competitive**
14.	**30**	29.05 ± 0.35	34.23 ± 0.27	**Non-competitive**
15.	**37**	57.04 ± 0.11	59.25 ± 0.41	**Non-competitive**
16.	**24**	55.01 ± 0.12	57.08 ± 0.16	**Non-competitive**
17.	**31**	30.01 ± 0.15	35.34 ± 0.34	**Non-competitive**
18.	**38**	44.21 ± 0.28	44.14 ± 0.13	**Non-competitive**
19.	**25**	46.13 ± 1.09	47.22 ± 0.11	**Non-competitive**
20.	**32**	32.01 ± 1.02	37.20 ± 0.16	**Non-competitive**
21.	**39**	53.17 ± 0.03	55.71 ± 0.05	**Non-competitive**
22.	**Glimepiride**	18.02 ± 0.015	23.02 ± 0.13	-

Experiments = 3, Values = mean ± SEM.

The substances exhibited strong scavenging abilities. With IC_{50} values of 49.15 ± 0.05 and 43.02 ± 0.13 (μM/mL) against DPPH, compounds **23** and **39** shown strong scavenging performance; in contrast, compounds **23** and **25** demonstrated exceptional efficacy against ABTS, with IC_{50} values of 29.01 ± 0.11 μM/mL and 29.01 ± 0.14 (μM/mL) respectively. The IC_{50} values of compounds **30** and **25** were 43 ± 0.09 μM/mL and 44 ± 0.15 (μM/mL), respectively, indicating their effectiveness in scavenging superoxide anion radicals (Tables 5–6). The scavenging activities of the other compounds were mild to moderate. Oxygen is crucial for life, but excess reactive oxygen species can cause serious health issues. Antioxidant drugs combat these problems through diverse mechanisms, and tests like DPPH, ABTS, and superoxide anion assays help evaluate their effectiveness and mechanisms [65–67]. Synthesized compounds show potent antioxidant effects, valuable for preventing oxidative stress-related disorders.

3.6. Structure optimizations and FMO analyses

FMO analysis is a key tool in quantum chemistry, focusing on a molecule's HOMO and LUMO [68]. It's vital in medicinal chemistry for predicting reactivity, selectivity, and electronic properties of drugs, aiding in identifying crucial molecular interactions for binding affinity and pharmacophore features [69]. For the analysis of MOs of the screened compounds, the structures were first energy minimized by employing MM2 force field which resulted the structural arrangement so that both homocyclic ring systems on the central nitrogen atom of sulfonamide moiety stay parallel one above the other along the mutual interactions of aromatic π clouds in compounds **21**, **22**, **24**, and **25** where the heterocyclic thiazole moiety stays away from these carbocyclic systems. In all the screened compounds **21**, **22**, **24**, **25**, **32**, and **38**, the electronic densities of HOMOs stay at the thiazole ring whereas the electronic densities of LUMOs stay at both of the carbocyclic ring systems with head on overlaps of MOs of the two ring systems for compounds **21**, **22**, **24**, and **25**, whereas, the derivatives **32** and **38** contain one carbocyclic ring which held the electronic density (Fig. 1). It was found that the electronic cloud stays on the carbocyclic moieties in the excited state of **22** and as it is electronically rich part which resultantly attracted the acidic amino acid Asp730 through a π-cation force in the docked complex. Moreover, as the carbocyclic rings overlapped over each other in the FMO structures thus rendering the $–SO_2-$ moiety more exposed which easily formed two intermolecular hydrogen bonds through its both oxygen atoms with the neighboring amino acids including Arg150, Ser209, Thr211, Lys716, Met746, thus suggesting that the results of FMO analyses were supporting the binding capabilities of screened motifs with their biological targets.

Considering the energies of HOMOs and LUMOs and the energy gaps, it is related to the functional moieties conjugated with the π systems such as the energies of HOMO and LUMO for compound **22** with no substituent at the aromatic rings were found to be −5.783 eV and 0.022 eV with the energy gap of 5.805, whereas, bromo and fluoro at the para position increased this energy difference minutely by shifting LUMO to somewhat higher with energy values of 0.278 eV and 0.288 eV along with the energy gaps of 6.089 eV and 6.078 eV for compounds **21** and **24**, respectively. The presence of nitro functionality at the para positions of compound **25** and **32** sufficiently reduced the energy gaps to 0.384 eV and 1.187 eV by lowering the energies of LUMOs to −5.336 eV and −4.997, respectively (Table 7). As higher chemical reactivity and decreased stability are generally indicated by a smaller HOMO-LUMO energy gap, which might improve a compound's capacity to interact with biological targets. The compound **38** has the smallest HOMO-LUMO

Table 3
Concentration-dependent antioxidant effect of compounds **19**, **20**, **26**, **27**, **33**, and **34**.

	Compounds	Concentrations (μM)					IC_{50}, (μM/mL)
		25	50	75	100		
(a) Concentration-dependent DPPH % Scavenging	**19**	39.1 ± 0.2	65.8 ± 0.03	89.6 ± 0.11	95.1 ± 0.41		40.01 ± 0.01
	20	35.2 ± 0.1	49.2 ± 0.01	56.3 ± 0.83	80.2 ± 0.01		43.5 ± 0.03
	26	43.2 ± 0.8	74.8 ± 0.3	88.5 ± 0.1	99.2 ± 0.2		38.3 ± 0.03
	27	33.2 ± 0.01	59.6 ± 0.2	75.4 ± 0.2	91.8 ± 0.03		39.2 ± 0.02
	33	30.2 ± 0.2	37.4 ± 0.1	65.6 ± 0.01	88.3 ± 0.2		34.4 ± 0.07
	34	29.2 ± 0.01	69.6 ± 0.2	78.4 ± 0.2	94.8 ± 0.03		45.5 ± 0.05
	Ascorbic acid	48.2 ± 0.02	70.3 ± 0.01	85.3 ± 0.01	97.2 ± 0.2		30.4 ± 0.08
		10	**20**	**30**	**40**	**50**	
(b) Concentration-dependent ABTS % Scavenging	**19**	18.01 ± 0.09	37.05 ± 0.04	41.09 ± 0.01	69.02 ± 0.03	89.03 ± 0.91	37.01 ± 0.04
	20	15.04 ± 0.2	22.02 ± 0.05	45.08 ± 0.06	61.01 ± 0.03	82.03 ± 0.07	38.01 ± 0.06
	26	09.02 ± 0.03	24.03 ± 0.01	43.08 ± 0.09	75.07 ± 0.02	96.06 ± 0.21	33.01 ± 0.09
	27	10.02 ± 0.05	19.08 ± 0.03	43.02 ± 0.09	70.02 ± 0.11	93.09 ± 0.02	40.05 ± 0.08
	33	29.02 ± 0.08	41.07 ± 0.03	49.08 ± 0.01	72.02 ± 0.07	113.03 ± 0.05	113.03 ± 0.05
	34	27.2 ± 0.01	35.6 ± 0.2	46.4 ± 0.2	69.8 ± 0.03	80.1 ± 0.08	47.05 ± 0.0
	Trolox	36.08 ± 0.1	58.02 ± 0.62	67.03 ± 0.02	85.01 ± 0.06	105.02 ± 0.02	16.4 ± 0.08
		25	**50**	**75**	**100**		
(c) Concentration-dependent superoxide anion % scavenging	**19**	32 ± 0.07	59 ± 0.25	80 ± 0.11	88 ± 0.01		42 ± 0.15
	20	31 ± 0.02	54 ± 0.12	79 ± 0.22	85 ± 0.25		40 ± 0.06
	26	27 ± 0.07	63 ± 0.01	73 ± 0.11	94 ± 0.51		36 ± 0.22
	27	25 ± 0.17	71 ± 0.25	86 ± 0.03	93 ± 0.52		45 ± 0.19
	33	20 ± 0.01	51 ± 0.03	60 ± 0.15	99 ± 0.18		38 ± 0.55
	34	18.2 ± 0.01	39.6 ± 0.2	69.4 ± 0.2	89.8 ± 0.03		52.1 ± 0.01
	Ascorbic acid	39 ± 0.09	55 ± 0.05	77 ± 0.12	90 ± 0.02		33.4 ± 0.08

Experiments = 3.
Values = mean ± SEM.

gap and is expected to be highly reactive towards it biological targets as it was found to be with better IC_{50} values of 24.31 ± 0.18, 27.15 ± 0.14, 44.21 ± 0.28, and 44.14 ± 0.13 against the J.B urease, B.P urease, glucosidase, and amylase enzymes which are found to be much better than many other similar compounds.

3.7. Physiochemical properties and drug likelihood

The rate and extent of drug absorption throughout the digestive process are determined by the intestinal absorption process, which makes it essential for the drug's effectiveness [70]. The screened compounds **21**, **22**, **24**, **25**, **32**, and **38** showed higher values of GI absorptions indicating their greater absorbability by the intestine with increased therapeutic outcomes because drug with little absorption in the GI tract may lead to reduced bioavailability, little or no therapeutic efficacy, and requirement of higher doses and resultantly increasing the risk of adverse effects. Another corresponding parameter for the measurement of bioavailability of a drug is the impact of P-gp on target ligands [71] and the measurement of this parameter for the screened motifs declared them to be non-substrates of this protein thus resulting the probability of higher concentrations of drug to reach the circulation system. The blood–brain barrier (BBB) prevents entry into the brain of most drugs from the blood [72]. The output values of all the screened compounds indicate them to be non-permeable of BBB thus declaring these ligands to be non-CNS drug candidates, reduction in the unintended effects on CNS, minimizing side effects on CNS such cognitive impairment, enhancing safety profile, and indicating them to be focused on their intended therapeutic targets permeability therefore all are not able to cross the blood-brain barrier. The rate at which a substance penetrates the stratum corneum is known as skin permeation, or Log Kp, and it represents an additional possible route for drug administration. This number is frequently used to quantify the movement of molecules in the epidermal skin's outermost layer and to highlight the importance of skin absorption. The Kp presents a measure by which the potential of biological uptake *via* the skin for a compound can be quantified and the datasets by QSPR evaluation of screened libraries of compounds resulted the skin

Table 4
Concentration-dependent antioxidant effect of compounds **21**, **22**, **28**, **29**, **35**,and **36**.

	Compounds	Concentrations (μM)					IC_{50}, (μM/mL)
		25	50	75	100		
(a) Concentration-dependent DPPH % Scavenging	**21**	35.1 ± 0.05	63.5 ± 0.11	90.5 ± 0.16	99.1 ± 0.32		45.2 ± 0.03
	22	31.4 ± 0.08	50.1 ± 0.11	66.1 ± 0.23	79.5 ± 0.05		57.2 ± 0.07
	28	48.2 ± 0.09	70.7 ± 0.01	85.3 ± 0.3	91.2 ± 0.06		48.4 ± 0.11
	29	34.5 ± 0.21	49.1 ± 0.13	77.2 ± 0.7	93.5 ± 0.08		52.5 ± 0.11
	35	28.1 ± 0.04	34.4 ± 0.8	61.5 ± 0.03	89.1 ± 0.6		53.1 ± 0.11
	36	25.3 ± 0.07	65.5 ± 0.12	88.3 ± 0.11	93.8 ± 0.09		49.3 ± 0.099
	Ascorbic acid	45.2 ± 0.01	68.2 ± 0.17	88.1 ± 0.02	94.2 ± 0.5		42.2 ± 0.06
		10	**20**	**30**	**40**	**50**	
(b) Concentration-dependent ABTS % Scavenging	**21**	15.1 ± 0.05	30.5 ± 0.04	46.03 ± 0.11	72.05 ± 0.15	90.03 ± 0.51	33.01 ± 0.05
	22	12.04 ± 0.01	27.2 ± 0.5	47.03 ± 0.06	66.11 ± 0.31	86.13 ± 0.12	40.01 ± 0.01
	28	10.01 ± 0.02	27.3 ± 0.05	48.08 ± 0.9	55.7 ± 0.22	99.06 ± 0.25	35.01 ± 0.11
	29	19.2 ± 0.5	23.07 ± 0.13	45.01 ± 0.19	74.12 ± 0.17	89.19 ± 0.12	43.21 ± 0.15
	35	33.02 ± 0.08	31.05 ± 0.01	43.01 ± 0.03	62.2 ± 0.09	105.13 ± 0.11	38.01 ± 0.13
	36	23.2 ± 0.11	37.5 ± 0.2	48.3 ± 0.21	65.5 ± 0.01	87.5 ± 0.05	45.07 ± 0.09
	Trolox	26.05 ± 0.03	55.02 ± 0.12	70.03 ± 0.01	82.01 ± 0.05	109.2 ± 0.22	19.4 ± 0.03
		25	**50**	**75**	**100**		
(c) Concentration-dependent superoxide anion % scavenging	**21**	33 ± 0.3	57 ± 0.13	82 ± 0.01	86 ± 0.11		45 ± 0.03
	22	35 ± 0.02	57 ± 0.15	80 ± 0.25	87 ± 0.15		40 ± 0.06
	28	25 ± 0.02	66 ± 0.11	77 ± 0.18	99 ± 0.31		39 ± 0.14
	29	28 ± 0.07	73 ± 0.20	85 ± 0.13	96 ± 0.32		43 ± 0.17
	35	27 ± 0.12	53 ± 0.05	64 ± 0.04	89 ± 0.28		38 ± 0.55
	36	20.6 ± 0.11	43.6 ± 0.12	65.1 ± 0.5	87.5 ± 0.08		57.1 ± 0.09
	Ascorbic acid	49 ± 0.05	53 ± 0.03	75 ± 0.15	93 ± 0.01		35.4 ± 0.19

Experiments = 3.
Values = mean ± SEM.

permeation values range between −11.436 cm/s and −1.778 cm/s with the majority of compound lying < −4 cm/s and >-10 cm/s [73]. The test compounds **21**, **22**, **24**, **25**, **32**, and **38** have log Kp values −5.83, −5.02, −5.88, −6.23, −6.54, and −6.48 respectively, representing their placements in the optimal range thus indicating these compounds drug-like and possess good dermal permeability and may be administered *via* the route alternative to oral path (Table 8).

QED scoring evaluates a compound's drug-likeness by considering factors like molecular weight, lipophilicity, polarity, and other physicochemical properties, aiding in drug discovery [74]. A greater QED score >0.67 corresponds to the attractive molecules in the process of drug discovery whereas the unattractiveness varies proportional to the decrease in this value. Among the screened compounds, the derivatives **22**, **24**, and **38** stood favorite with the QED scores of 0.719, 0.707, and 0.860, respectively, whereas the derivatives **21**, **25**, and **32** exhibited this value 0.631, 0.486, and 0.462, respectively. SA score is implemented based on the synthetic accessibility score, which is an estimated ease of synthesis of a drug-like molecule [75]. Drug-like molecules having SA score of ≥6 are difficult to synthesize, while those with a score of <6 are easy to achieve synthetically. The SA scores of all the compounds **21**, **22**, **24**, **25**, **32**, and **38** of 2.107, 2.096, 2.057, 2.185, 2.517, and 2.248 respectively were in the acceptable range of synthetic ease which were in accordance with the experimental data of synthesis of these motifs in better yields thus validating the model adopted for the computational studies. Another metric used in medicinal chemistry is Fsp^3 and its higher value is associated with increased water solubility, lower lipophilicity, and enhanced metabolic stability and thus improving bioavailability, reduction in toxicity, and enhanced drug-like properties, ultimately increasing the likelihood of success in the drug development process [76]. The compounds **21**, **22**, **24**, **25**, **32**, and **38** exhibited Fsp^3 values of 0.062, 0.087, 0.062, 0.062, 0.083, and 0.1 respectively thus establishing that the compounds **22**, **32**, and **38** had comparatively greater saturation in their structures than rest of the screened motifs. Caco-2 is a human epithelial colorectal adenocarcinoma cell line that is commonly used in drug discovery and development and widely used in absorption studies [77] with the optimal score for this assay to be > −5.15 log unit where all the screened compound stood in the optimal range

Table 5
Concentration-dependent antioxidant effect of compounds **23**,**24**,**30**,**31**,**37**and**38**.

	Compounds	Concentrations (μM)					IC_{50}, (μM/mL)
		25	50	75	100		
(a) Concentration-dependent DPPH % Scavenging	**23**	32.6 ± 0.21	57.3 ± 0.01	70.5 ± 0.16	93.05 ± 0.32		49.15 ± 0.05
	24	21.3 ± 0.18	44.1 ± 0.55	75.1 ± 0.30	89.4 ± 0.35		62.5 ± 0.07
	30	38.5 ± 0.19	46.1 ± 0.11	77.2 ± 0.13	81.2 ± 0.15		52.3 ± 0.21
	31	34.02 ± 0.1	43.1 ± 0.13	73.2 ± 0.5	90.5 ± 0.11		66.3 ± 0.2
	37	19 ± 0.17	42.4 ± 0.8	66.8 ± 0.15	99.1 ± 0.21		57.1 ± 0.11
	38	21.3 ± 0.11	67.3 ± 0.2	89.3 ± 0.05	95.01 ± 0.9		69.5 ± 0.1
	Ascorbic acid	20.2 ± 0.11	58.1 ± 0.05	79.1 ± 0.12	84.2 ± 0.18		45.11 ± 0.16
		10	**20**	**30**	**40**	**50**	
(b) Concentration-dependent ABTS % Scavenging	**23**	19.5 ± 0.05	39.5 ± 0.24	55.13 ± 0.13	76.01 ± 0.5	93.03 ± 0.31	30.01 ± 0.11
	24	25.11 ± 0.11	33.6 ± 0.55	44.31 ± 0.17	48.23 ± 0.51	76.23 ± 0.22	42.12 ± 0.21
	30	23.11 ± 0.02	40.3 ± 0.53	46.01 ± 0.19	59.5 ± 0.20	87.11 ± 0.15	37.6 ± 0.01
	31	29.31 ± 0.2	37.15 ± 0.28	41.11 ± 0.39	47.12 ± 0.17	73.04 ± 0.12	46.13 ± 0.13
	37	30.22 ± 0.22	41.25 ± 0.11	48.01 ± 0.12	65.5 ± 0.07	99.03 ± 0.15	34.11 ± 0.16
	38	13.2 ± 0.91	35.3 ± 0.42	41.2 ± 0.71	48.13 ± 0.11	79.3 ± 0.44	49.03 ± 0.15
	Trolox	35.01 ± 0.3	65.2 ± 0.1	77.31 ± 0.07	89.01 ± 0.5	105.12 ± 0.21	17.5 ± 0.05
		25	**50**	**75**	**100**		
(c) Concentration-dependent superoxide anion % scavenging	**23**	39 ± 0.3	60 ± 0.56	89 ± 0.07	103 ± 0.19		47 ± 0.11
	24	33 ± 0.21	45 ± 0.35	84 ± 0.25	97 ± 0.15		59 ± 0.16
	30	29 ± 0.34	63 ± 0.01	79 ± 0.11	87 ± 0.21		43 ± 0.09
	31	25 ± 0.11	46 ± 0.05	79 ± 0.33	104 ± 0.22		60 ± 0.05
	37	37 ± 0.21	43 ± 0.6	67 ± 0.03	99 ± 0.15		54 ± 0.15
	38	31.5 ± 0.11	45.01 ± 0.5	55.7 ± 0.5	92.5 ± 0.03		67.6 ± 0.93
	Ascorbic acid	35 ± 0.33	57 ± 0.13	86 ± 0.53	99 ± 0.11		39.1 ± 0.21

No. of experiments = 3.
Values presented are mean ± SEM.

Table 6
Concentration-dependent antioxidant effect of compounds **25**, **32** and **39**.

Compounds	Concentrations (μM)					IC_{50}, (μM/mL)
	25	**50**	**75**	**100**		
25	35.2 ± 0.2	57.8 ± 0.11	71.6 ± 0.03	85.1 ± 0.41		47.1 ± 0.08
32	39.2 ± 0.2	53.5 ± 0.3	64.4 ± 0.01	88.2 ± 0.2		46.2 ± 0.01
39	15.04 ± 0.05	55.02 ± 0.08	77.08 ± 0.11	91.01 ± 0.34		43.02 ± 0.13
Ascorbic acid	43.2 ± 0.02	69.3 ± 0.41	95.3 ± 0.01	105.2 ± 0.2		35 ± 0.05
	10	**20**	**30**	**40**	**50**	
25	09.01 ± 0.09	28.05 ± 0.04	43.09 ± 0.01	70.02 ± 0.03	81.03 ± 0.91	29.01 ± 0.14
32	12.02 ± 0.03	25.03 ± 0.01	49.01 ± 0.09	75.03 ± 0.02	94.06 ± 0.21	31.01 ± 0.09
39	24.02 ± 0.05	39.01 ± 0.3	47.06 ± 0.1	72.11 ± 0.09	102.03 ± 0.01	36.09 ± 0.15
Trolox	18.08 ± 0.1	40.02 ± 0.62	55.03 ± 0.02	84.01 ± 0.06	93.02 ± 0.02	20.3 ± 0.02
	25	**50**	**75**	**100**		
25	19 ± 0.07	25 ± 0.25	44 ± 0.10	67 ± 0.01		44 ± 0.15
32	15 ± 0.05	32 ± 0.02	67 ± 0.11	97 ± 0.51		49 ± 0.12
39	22.2 ± 0.01	48.5 ± 0.17	71.4 ± 0.34	93.8 ± 0.11		54.1 ± 0.55
Ascorbic acid	25 ± 0.03	60 ± 0.07	67 ± 0.11	82 ± 0.01		38 ± 0.20

Experiments = 3.
Values = mean ± SEM.

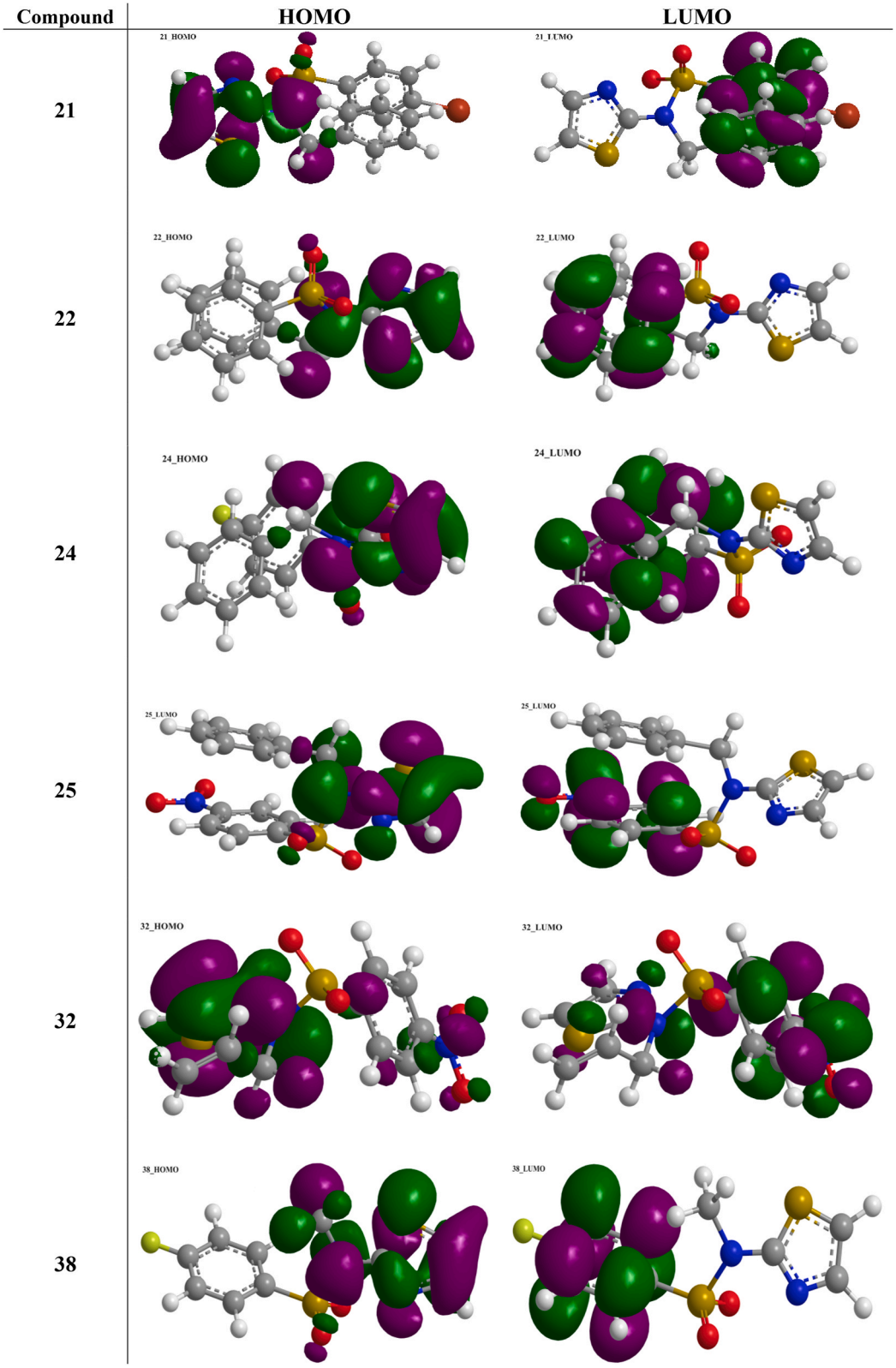

Fig. 1. Surface plots of molecular orbitals of compounds **21**, **22**, **24**, **25**, **32**, and **38**.

Table 7
Energies of HOMOs and LUMOs of compounds **21**, **22**, **24**, **25**, **32**, and **38** along with HOMO-LUMO energy differences.

Compound	HOMO (eV)	LUMO (eV)	Eg(eV)
21	−5.811	0.278	6.089
22	−5.783	0.022	5.805
24	−5.790	0.288	6.078
25	−5.720	−5.336	0.384
32	−6.184	−4.997	1.187
38	−5.960	0.349	6.309

Table 8
Absorption and bioavailability potential of screened motifs **21**, **22**, **24**, **25**, **32**, and **38**.

Compound	GI absorption	BBB permeant	P-gpsubstrate	Log Kp (skin permeation)	Bioavailability score
21	High	No	No	−5.83	0.55
22	High	No	No	−5.84	0.55
24	High	No	No	−5.88	0.55
25	Low	No	No	−6.23	0.55
32	Low	No	No	−6.54	0.55
38	High	No	No	−6.48	0.55

with −4.664, −4.924, −4.615, −4.707, −4.567, and −4.235 Caco-2 Permeability scores for the compounds **21**, **22**, **24**, **25**, **32**, and **38**, respectively. The Madin–Darby canine kidney (MDCK) permeability is another parameter useful to assess BBB permeability, oral bioavailability, drug transporter interactions, and for drug regulatory purposes [78]. The standard low, medium, and high passive permeability scores are distributed to $<2 \times 10^{-6}$ cm/s, 2–20 $\times 10^{-6}$ cm/s, and $>20 \times 10^{-6}$ cm/s, respectively. Among the screened compounds, exhibited high passive permeability with 1.70 x 10^{-5}, 2.40 x 10^{-5}, 2.13 x^{-5}, 1.29 x 10^{-4}, 1.50 x 10^{-4}, and 2.53 x 10^{-5}, respectively, indicating their improved absorptions, greater concentrations of drug reaching circulation system, and more desirable pharmacokinetics profiles.

The optimal range of Plasma protein binding (PPB) is <90 % because highly protein-bound drugs may have a low therapeutic index. High plasma protein binding limits the partitioning of xenobiotics from the blood into the tissues where they could be metabolized. This serves to extend the half-life of the xenobiotic as only free chemicals may enter the metabolizing enzymes [79]. All the compounds have PPB values higher than the optimal range. High PPB values may affect the drug's clinical results. Thus, amendments will be made to set the PPB value.

MCE-18 stands for medicinal chemistry evolution. The optimum MCE-18 score limit given by ADMETlab 2.0 is ≥ 45. **A1**, **A2**, **A3**, **A4**, **A5**, and **A6** have MCE-18 scores of 17, 21, 17, 18, 14, and 13 respectively. All the values are below the optimum range.

NP score reflects the natural product-likeness score. This score ranges from −5 to 5; the higher the score, the higher the probability of being a natural product. Natural products are more likely to be safe, with reduced risk of toxicity. All the values −1.96,-1.416,-2.176,-2.097,-2.308, and-2.442 lie in the optimal range (Table 9).

The human Ether-a-go-go-Related Gene (hERG) K^+ channel blockade is linked with fatal cardiac arrhythmias. Preventing severe cardiac adverse effects, guaranteeing the safety of pharmaceutical compounds, and increasing the overall success rate of drug development all depend on designing medications with lower hERG liability [80]. Among the screened compounds, the hERG values were found to be 0.033, 0.017, 0.028, 0.137, 0.024, and 0.008 for compounds **21**, **22**, **24**, **25**, **32**, and **38** which were approaching to zero thus indicating the safety of these drug candidates for cardiovascular system. The probabilities of the screened motifs for the inhibition of CYP1A2 estimated by the employed algorithm were 0.724, 0.750, 0.711, and 0.738 for **21**, **22**, **24**, and **38** indicating them to be better inhibitors whereas the compounds **25** and **32** offered moderate inhibitory potentials of 0.586 and 0.629, respectively. Similarly, the screened compounds were found to be poor substrates of this enzyme with 0.368, 0.235, 0.387, 0.114, and 0.270, respectively except compound **38** with the value of 0.756 indicating it to be more vulnerable for biotransformation by this enzyme. The probabilities of the screened compounds **21**, **22**, **24**, **25**, **32**, and **38** to inhibit CYP2C19 estimated to be 0.974, 0.95, 0.975, 0.971, 0.939, and 0.939 respectively declared these derivatives to be potent inhibitors of this metabolic enzyme whereas this protein was moderately active to bio transform the most of these compounds as substrates except **38** with the score of 0.866 being more vulnerable

Table 9
Drug permeation investigations of compounds **21**, **22**, **24**, **25**, **32**, and **38**.

No.	QED	SA score	Fsp3	MCE-18	NP score	Caco-2 Permeability	MDCK Permeability	PPB
21	0.631	2.107	0.062	17	−1.96	−4.664	1.70E-05	98.15 %
22	0.719	2.096	0.062	16	−1.897	−4.768	2.40E-05	97.84 %
24	0.707	2.057	0.062	17	−2.176	−4.615	2.13E-05	98.20 %
25	0.486	2.185	0.062	18	−2.097	−4.707	1.29E-04	98.20 %
32	0.462	2.517	0.083	14	−2.308	−4.567	1.50E-04	95.11 %
38	0.860	2.248	0.1	13	−2.442	−4.235	2.53E-05	95.60 %

to the biochemical modifications. Moreover, all the investigated compounds were found to be good CYP2C9 inhibitors due to their higher probability values of 0.969, 0.967, 0.965, 0.963, 0.913, and 0.899. CYP3A4, the primary and most clinically significant drug-metabolizing enzyme in the human body, oxidizes more than 50 % of commonly used medications; however, some of these substances also function as inducers, effectors, and inhibitors of CYP3A4. On the other hand, these compounds were also effective CYP2C9 substrates. Inhibition of CYP3A4 is generally undesirable and can result in drug toxicity, drug-drug interactions, and other negative effects. CYP3A4 inactivation, however, may be advantageous in some circumstances since it may increase the therapeutic efficacy of medicines that are rapidly digested by raising their plasma levels. In this study, the compounds **A1**, **A2**, **A3**, and **A4** with probability values of 0.833, 0.862, 0.813, and 0.835, respectively, were good CYP3A4 inhibitors and **A5** as a moderate inhibitor as its value is 0.656. However, the compound **A6** was found to be a poor inhibitor as it has a very low value of 0.177, whereas, the rest of the characteristics of screened candidates are presented in Table 10. In conclusion, these investigations offer an overview of behaviors of synthesized compounds in the human metabolic system, as drug candidates.

3.7.1. Metabolism evaluation

When drugs enter the body, the liver metabolizes them through various processes like hydrolysis, condensation, conjugation, oxidation, reduction, and isomerization. These transformations break down the drugs into metabolites, some of which are pharmacologically active and contribute to the medication's effects. However, the metabolism rate varies among individuals, affecting the drug's efficacy and toxicity.

The metabolites were obtained by the metabolic processes the parent compound **21** has undergone various reactions and thus different metabolites have been obtained. The metabolite **M1** was obtained by the aromatic hydroxylation of the parent compound and the probability of this predicted biotransformation to undergo in the real biological system was found to be 0.9313, **M2** by aromatic hydroxylation with 0.7832 probability, **M3** by aromatic hydroxylation with a 0.9505 probability rate, **M4** was obtained by the glutathionation reaction of the parent compound with probability rate of 0.9974, **M5** was obtained by *S*-oxidation of the parent compound with probability of 0.9980, **M6** metabolite was obtained by the reaction *N*-dealkylation of the parent compound with probability rate of 0.9851.

The physiological potencies of the parent compound **21** and its predicted metabolites were evaluated by the employed algorithm which declared the parent compound to be active as an ABCA1 expression enhancer, transcription factor inhibitor and β-lactamase inhibitor with activity (Pa) values of 0.556, 0.482, and 0.325 respectively, where some of the predicted metabolites also showed some activity for these factors with Pa values with slight variations such as **M1** shows activity as ABCA1 expression enhancer (Pa = 0.511) and transcription factor inhibitor (Pa = 0.472) which were comparable to the parent compound, **M2** also showed the activity against these proteins with Pa scores of 0.510 and 0.493 respectively, the Pa value for the transcription factor inhibitor is slightly greater which shows that the **M2** shows greater activity for transcription factor inhibitor as compared to the parent compound and the **M1**. **M3** was also found to be ABCA1 expression enhancer and transcription factor inhibitor with the Pa values of 0.522 and 0.462 respectively, where the rest of the metabolites were less active in the physiological responses. The metabolite **M4** was also mildly active as Glutathione S-transferase inhibitor and Cyclin-dependent kinase 2 inhibitor with Pa values of 0.271 and 0.265, respectively. **M1**, **M2**, and **M3** were mild lipoxygenase inhibitors with the activity scores of 0.394, 0.414, and 0.363. The metabolic product **M5** was a potent analgesic with a Pa value of 0.784, an anti-inflammatory candidate with a Pa value of 0.730, and an antioxidant with a Pa value of 0.562. The metabolite **M7** showed various potentials as Nav1.3 sodium channel blocker, sodium channel blocker, and Nav1.5 sodium channel blocker with the Pa values of 0.709, 0.569, and 0.533, respectively.

During the toxicity evaluations, most of the metabolites showed very little toxicity in the body causing only few toxic side effects such as the parent compound showed the toxicity of ulceration with a Pa value of only 0.114. On the other hand, **M1**, **M3**, **M4**, **M5**, and **M6** also showed similar toxicity with minor variations as the ulceration toxicity score for **M1** was found to be 0.120 which is nearly similar to the parent compound, **M3** and **M6** had ulceration toxicity by 0.119 and a 0.117 value reflecting that there is also somehow little toxicity by these metabolites, **M4** had extraordinarily reduced ulceration toxicity with Pa score of only 0.044 which is even less than the parent compound as well as other metabolites. Similarly, the metabolite **M5** exhibited ulceration toxicity less than the parent moiety with Pa value of 0.132. Further, the parent compound also showed the toxicity of carcinogenic group 1 with a Pa score of only 0.067 indicating its little or no carcinogenicity. Other metabolites **M1**, **M2**, **M3**, **M4**, **M5**, and **M6** all showed the toxicity of carcinogenic group 1 with Pa scores of 0.063, 0.061, 0.066, 0.028, 0.067, and 0.076 respectively. Out of these investigations, **M4** showed least toxicity in this category with a Pa score of 0.028 whereas all other metabolic products had Pa values a little higher than **M4** with few variations. Further screening of parent compound showed some little toxicity of pneumotoxic with 0.042 Pa value, **M2** also showed pneumotoxicity in an acceptable range with Pa value of 0.061, minutely higher than the parent compound, **M5** was also found to be

Table 10
Enzymatic metabolism investigation of screened compounds **21**, **22**, **24**, **25**, **32**, and **38**.

Compound	CYP1A2-inh/sub	CYP2C19-inh/sub	CYP2C9-inh/sub	CYP2D6-inh/sub	CYP3A4-inh/sub	hERG	Ames	NR-PPAR-gamma
21	0.724/0.368	0.974/0.649	0.969/0.935	0.627/0.358	0.833/0.92	0.033	0.031	0.216
22	0.750/0.235	0.979/0.643	0.967/0.854	0.451/0.249	0.781/0.922	0.017	0.023	0.449
24	0.711/0.387	0.975/0.503	0.965/0.929	0.616/0.427	0.813/0.918	0.028	0.042	0.673
25	0.586/0.114	0.971/0.393	0.963/0.953	0.58/0.511	0.835/0.915	0.137	0.718	0.273
32	0.629/0.270	0.939/0.603	0.913/0.943	0.703/0.807	0.656/0.834	0.024	0.939	0.042
38	0.738/0.756	0.939/0.866	0.899/0.928	0.15/0.52	0.177/0.91	0.008	0.089	0.336

safe with a Pa score of 0.047. The metabolites **M1**, **M2**, **M3**, and **M6** all are very safe to be metabolized in the body, they exhibit little or no hypoglycemic with Pa scores of 0.088, 0.071, 0.081, and 0.155 respectively, only **M6** have very little potential to cause hypoglycemic otherwise there is no such toxicity to be concerned (Fig. 2).

Another algorithm [81] was employed for the prediction of metabolic outcomes of compound **21** after its absorption as a drug candidate resulting various metabolites among which **E1** and **E2** were obtained by the environmental microbial transformation of the parent moiety, bearing the ALogP values of 3.3179 and 3.1049 respectively reflecting that they were polar compounds. The metabolites **AB1**and **AB2** were obtained by the hydrolysis of sulfonamide moiety to sulfonic acid and the corresponding secondary amine by

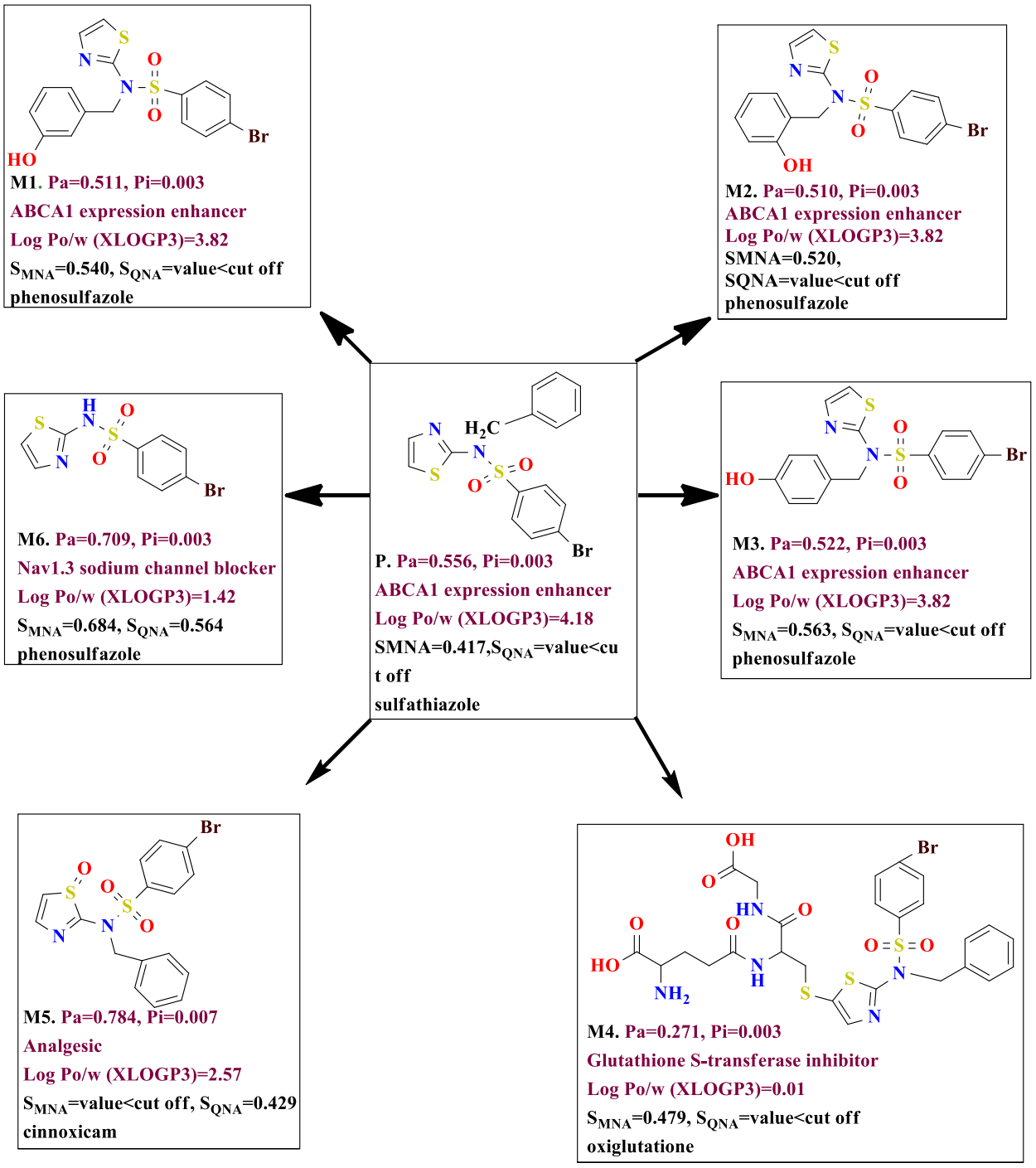

Fig. 2. Schematic representation of formation of metabolite of compound **21** with calculated Pa/Pi scores, LogP, and drug likeness.

an abiotic transformation, with ALogP values of 1.5418 and 2.2194, respectively. **AB3** (ALogP = 0.9651) were obtained by sulfonamide *C-S*photo hydrolysis of the parent compound by an abiotic transformation, whereas **AB4** and **AB5** metabolites were also obtained by an abiotic transformation process, the parent moiety underwent ozonation by the oxidation of para position of the substrate,

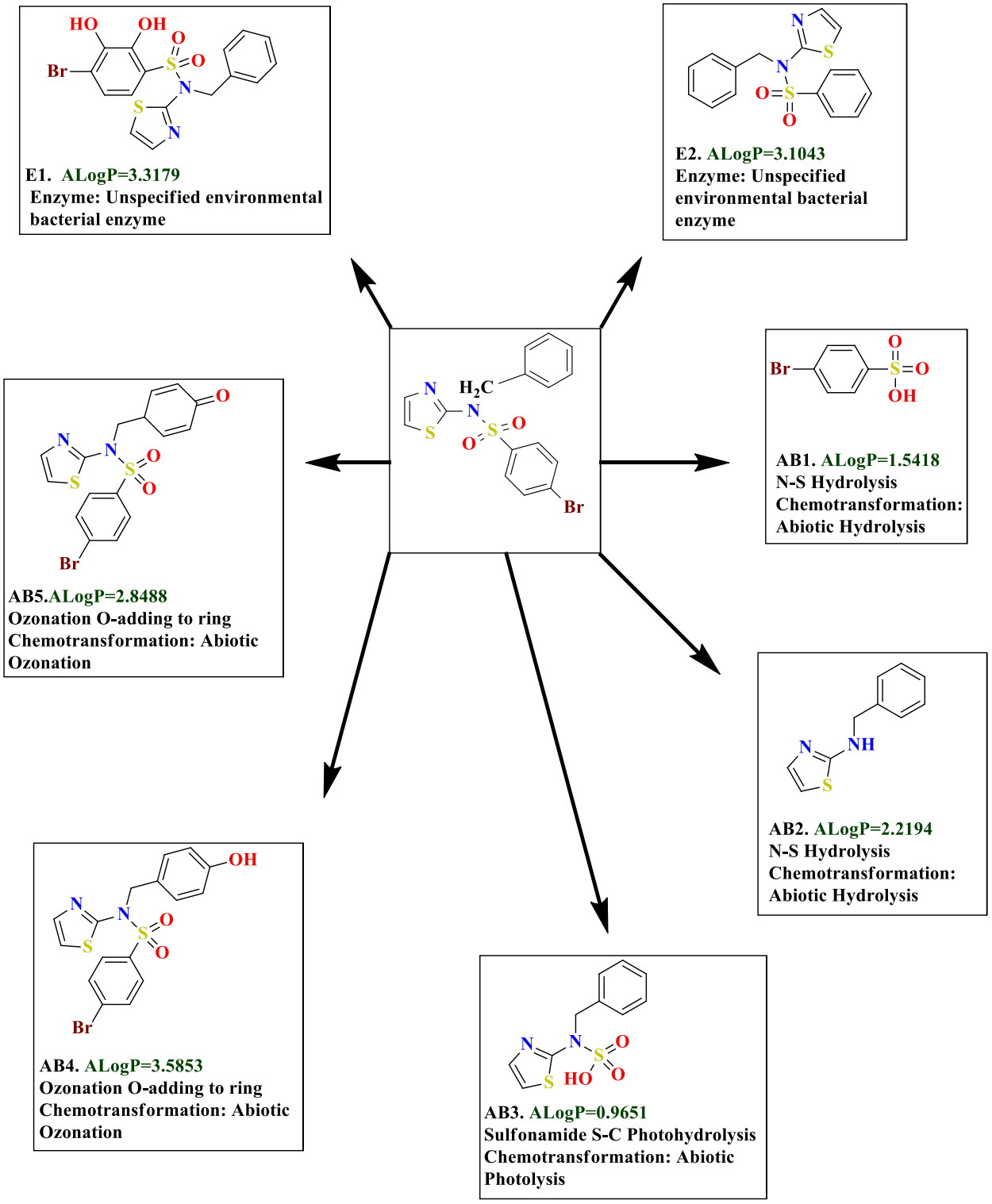

Fig. 3. Schematic representation of fragmentation pattern and resulting metabolites of compound **21** with calculated ALogP, reaction type and fragmenting enzymes.

with ALogP values of 3.5853 and 2.8488, respectively.

Investigations on the drug resemblance of these metabolic products, it was found that **E1** had a structure resemblance with some marketed drugs, firstly with *N*-[4-(aminosulfonyl)benzyl]-5-(5-chloro-2,4-dihydroxyphenyl)-1*H*-pyrazole-4-carboxamidewith a resemblance score of 0.202, with xipamide with a score of 0.143. **E2** had similarities with *N*-butyl-benzenesulfonamide with a score of 0.309, the drugsfamphur and 2, 2′-dibenzothiazyl disulfide also showed similarity with the metabolite **E2** with similarity scores of 0.203 and 0.158, respectively. Further, **AB1** metabolite had similarity with the approved drugs 2-naphthalenesulfonic acid, *p*-toluenesulfonic acid, and 5-(dimethylamino)-1-naphthalenesulfonic acid (dansyl acid) with similarity scores of 0.989, 0.982, and 0.951. Similarly, **AB2** had similarity with drugs 5-benzyl-1,3-thiazol-2-amine, Ñ3∼-benzylpyridine-2,3-diamine, and thiabendazole with a score of 0.876, 0.829, and 0.791, whereas, the metabolite **AB3** had similarity with the drug nitazoxanide(a thiazolide anti-infective used to treat infections by protozoa, helminths, anaerobic bacteria, microaerophilic bacteria, and viruses) and 2-amino-*N*-(4-methyl-1,3-thiazol-2-yl)-5-[(4-methyl-4*H*-1,2,4-triazol-3-yl)sulfanyl]benzamide with a score of 0.776 and 0.685. Moreover, **AB4** exhibited similarity with the drugs2-amino-*N*-(4-methyl-1,3-thiazol-2-yl)-5-[(4-methyl-4*H*-1,2,4-triazol-3-yl)sulfanyl]benzamide and 2-(methylamino)-N-(4-methyl-1,3-thiazol-2-yl)-5-[(4-methyl-4H-1,2,4-triazol-3-yl)sulfanyl]benzamide with similarity scores of 0.500 and 0.479. Finally, **AB5** had resemblance with the standard drug 1-{3-[(4-pyridin-2-ylpiperazin-1-yl)sulfonyl]phenyl}-3-(1,3-thiazol-2-yl)urea with a score of 0.487 (Fig. 3).

3.8. Molecular dockings

Predicting protein-ligand binding compatibility *via* in silico methods has long been crucial in structure-based drug design. Now, relative binding free energy (RBFE) calculations, rooted in molecular simulations and statistical mechanics, offer a novel approach to this endeavor [82]. Binding free energy is the total of all the intermolecular interactions that are present between the ligand and the target. Binding free energy is the sum of all intermolecular interactions between the ligand and the target. Best-docked compounds showed binding energies from −8.0 to −11.71 kcal/mol. The compounds **21**, **22, 24, 25, 32,** and **38** exhibited binding energies of −7.03, −7.35, −6.63, −7.63, −6.75, and −5.75 kcal/mol, respectively. The ligand efficiency values of compounds **21**, **22, 24, 25, 32,** and **38** are −0.31, −0.25, −0.29, −0.31, −0.32, and −0.34 kcal/mol, respectively (Table 11). The inhibitory constant indicates a compound's ability to reduce the binding affinity of a ligand, affecting its partner's binding activity. It reflects the concentration at which the inhibitor occupies 50 % of receptor sites when no other ligands compete. Values for screened motifs ranged from 2.56 to 61.27 μM, with lower values indicating higher binding affinity and requiring less ligand to inhibit partner activity.

After closely examining the ligand-substrate complex of compound **21**, it was possible to identify three types of bonding: π-alkyl (4.66) between the heterocyclic ring's π-cloud and Val744's beta-carbon; π-alkyl (5.38) between the ring's π-cloud and Val36's β-carbon; and π-sulfur (5.84 Å) between Tyr32's π-cloud of the benzene ring and the sulfur contained in the ring. The benzene ring adjacent to the methyl (–CH_2–) group in the ligand, the π-π stacked (3.76 Å) interaction between the π-cloud of the ring and the π-cloud of the phenyl ring of Phe712, the π-alkyl (4.70 Å) bonding between the π-cloud of the ring and the γ-carbon of Lys716, the π-π stacked (5.47 Å) bonding between the π-cloud of the ring and the π-cloud of other benzene ring present within the ligand molecule, and a π-anion (3.78 Å) between the π-cloud of the ring and the terminal hydroxyl group of Asp730 will all be discussed now. The oxygen of the sulfonamide and the α-carbon of Lys745 were implicated in certain interactions between the ligand molecule and the sulfonamide group. The phenyl ring of the benzene sulfonamide moiety forms a π-alkyl (3.52 Å) interaction with the α-carbon of Lys716, a π-cation (4.76 Å) between the π-cloud of ring and the terminal amidic NH of Lys716, a π-alkyl (4.67 Å) between the π-cloud of ring and the sulfur atom found in Met746, the bromide present on the ring at para position formed an alkyl interaction with the sulfur atom of Met746 at the bond distance of 5.08 Å, an interaction (4.01 Å) with the five-membered ring of Pro717, and another interaction (4.01 Å) with the γ-carbon of Lys716.Ser 422, Glu 418, Phe712, Phe 838, Ser 421, Gly 641, Lys 709, and Tyr837 were discovered to be present in the binding pocket along with interacting amino acids in the case of compound 22's ligand-protein complex. The five-membered heteroatomic ring interacted with the following: the π-sulfur force (5.76 Å) connected the sulfur atom in the ring to the π-cloud of Tyr32's benzene ring; the π-sigma bonding (3.99 Å) linked the π-cloud of the five-membered unsaturated ring to the terminal methyl of Thr33; the carbon linkage (3.28 Å) linked the carbon atom adjacent to the nitrogen in the ring and the oxygen atom of the hydroxyl group of Thr33; and the conventional hydrogen bonding (3.28 Å) connected the nitrogen atom of the heterocyclic ring to the hydrogen of the terminal amidic –NH_2 of Lys716 with a bond distance of 2.13 Å. More details about the docked ligands and their interactions with the amino acid residues in the binding pocket of target substrates are given in Table 12.

Ligand-substrate complex of compound **24** featured significant interactions involving the five-membered hetero aromatic ring.

Table 11
Binding energy parameters of best docked conformations of the screened compounds **21**, **22, 24, 25, 32,** and **38** against urease enzyme PDB ID: 3LA4.

Compounds	Binding energy (Kcal/mol)	Ligand efficiency (Kcal/mol)	Inhib constant (μM)	Intermol energy	Vdw hb_desolv_energy	Electrostatic energy	Total internal	Torsional energy
21	−7.03	−0.31	7.01	−8.52	−8.58	0.06	−1.4	1.49
22	−7.35	−0.25	4.11	−9.44	−9.12	−0.31	−1.55	2.09
24	−6.63	−0.29	13.85	−8.12	−7.72	−0.4	−1.13	1.49
25	−7.63	−0.31	2.56	−8.52	−6.93	−1.59	−0.76	0.89
32	−6.75	−0.32	11.34	−7.64	−6.08	−1.57	−0.48	0.89
38	−5.75	−0.34	61.27	−6.64	−6.41	−0.24	−0.53	0.89

These interactions included a π-anion interaction (3.39 Å) between the aromatic ring's π-cloud and Asp730's terminal hydroxyl group, as well as a π-alkyl bonding (4.66 Å) with Lys716's α-carbon. The π-alkyl force (4.74 Å) between the π-cloud of the phenyl ring and the sulfur atom of Met746; the π-alkyl interaction (3.92 Å) between the π-cloud of ring and the γ-carbon of Lys716; and the π-cation force (4.76 Å) between the π-cloud of ring and the nitrogen of amidic NH_2 of Lys716 were among the prominent interactions among which the π cloud of benzyl moiety was involved. In the benzene sulfonamide portion, the third ligand ring formed a π-σ force (3.74 Å) between the π-cloud of ring and the terminal methyl group of Thr33, a π-alkyl interaction (4.61 Å) between the π-cloud of ring and the β-carbon of Val36, and an interaction between the hydroxyl group of Glu742 and the fluorine present at the para position of this benzene ring. Compounds **21**, **22**, **24**, **25**, **32**, and **38**'s ligand-protein complexes are depicted in three dimensions in Fig. 4, which displays each compound's complete binding patterns in its corresponding binding cavity.

3.9. MD simulations

Molecular Dynamics (MD) simulations are crucial for drug discovery, revealing how biological molecules behave at the atomic level. They model atom movements over time, offering insights into protein structures and interactions, aiding in identifying therapeutic opportunities [83,84]. MD simulations aid in optimizing drug design, assessing effectiveness, and predicting how drugs bind to target molecules where this guidance informs the development of new therapeutic agents [85]. The increased concentration of ammonia due to the action of urease enzyme along with the pH elevation result in negative implications in medicine and agriculture including urinary catheter encrustation, hepatic coma urolithiasis, pathologies induced by *Helicobacter pylori*, and pathogenesis of hepatic encephalopathy thus declaring this protein to be an important drug target [86]. Thus, the search of new urease inhibitors is still on for the development of novel inhibitors of this metalloenzyme with promising level of potency. In the enthusiasm of finding potential candidate inhibitors of an enzyme, molecular dynamic simulation explores the stability of ligand-protein complexes through the investigation of protein folding, flexibility of protein and ligand, protein-ligand binding interactions, and conformational changes in proteins after binding the ligand molecule [87].In drug discovery, stability of a ligand-protein complex as estimated by MD simulations is essential to guarantee high binding affinity, specificity, and efficacy which directs rational drug design, impacts pharmacodynamics, and helps overcome drug resistance [88].

3.9.1. Root mean square deviation (RMSD)

In drug development, a crucial metric for assessing molecular interactions is the computed residual RMSD of a ligand-protein complex, indicating precision and stability [89]. The structural variation in the expected locations of the atoms of complex is quantified by RMSD [90]. Predicting how a ligand binds to its target protein is vital in optimizing drug design. A low residual RMSD validates computational models, ensuring alignment with real biological systems. This knowledge refines molecular docking studies, enhancing ligand structures for improved binding affinity and specificity [91]. RMSD values of amino acid residues were calculated over a 175 nm simulation trajectory for three ligand-protein complexes: compounds **21**, **22**, and **24**. Plots with color-coded protein structures are depicted in the figure. Among the calculated data it was observed that the RMSD values ranged from 0.094 Å for Val 816 to 0.517 Å for Asn 297 with an average value of 0.243 Å per residue, from 0.103 Å for Gly 538 to 0.486 Å for Glu 598 with an average value of 0.241 Å, and from 0.092 Å for Gly 754 to 0.567 Å for Asn 836 with an average value of 0.239 Å per residue for the complexes of compounds **21**, **22**, and **24**, respectively, with the target substrate. The color-coded representations of protein structures along each plot differentiate between the portions with the little coded with blue, average coded with green and higher than average mobility coded with red, of amino acid residues. However, it is obvious form the MD simulation data of RMSD that the screened ligands formed stable complexes with the target substrate under the employed conditions and validates the reliability of the simulation model (Fig. 5).

3.9.2. Root mean square fluctuation (RMSF)

In MD simulations for drug development, estimation of RMSF plays a critical role by providing information on the flexibility of protein structures [92]. A dynamic profile of atomic fluctuations may be obtained by analyzing RMSF, which helps to identify the conformationally unstable areas of macromolecule [93]. Understanding the flexibility of binding sites is crucial for designing ligands

Table 12
Tabular depiction of Interacting Amino Acids (IAAs) and their Hydrophobic Interactions (HPIs) with the ligands docked in the binding cavities of the target protein.

Compound	IAAs	HPIs (Å)
21	Tyr32, Val 36, Phe712, Lys716, Pro717, Asp730, Val744, Lys745, Met746,	π-anion (4.20), π-cation (6.43), π-sulfur (6.65), π-π stacked (5.34), van der Waals (5.15), π-alkyl (4.12, 4.15, 4.49, 4.62, 4.97, 5.15, 5.34)
22	Tyr32, Thr33, Lys716, Asp730, Met746	Conventional hydrogen bonds (4.45, 5.53, 5.82), π-anion (4.45), π-cation (5.11, 6.99),π-sulfur (6.31), π-σ (5.46), van der Waals (3.87, 4.39),π-alkyl (4.89, 5.02)
24	Thr33, Val36, Lys716, Asp730, Glu742, Met746,	Conventional hydrogen bonds (4.50, 4.81),π-anion (4.53), π-cation (5.94),π-σ (4.41), van der Waals (4.72), π-alkyl (4.72, 4.87, 6.14), halogen (5.10)
25	Asn 193, Ile194, Val200, Lys208, Thr211	Conventional hydrogen bonds (4.18, 4.99), π-σ (4.90, 5.03), van der Waals (4.50), π-alkyl (6.61)
32	Ile 148, Arg150, Leu 308	Conventional hydrogen bonds (3.62, 5.47),π-alkyl (4.76, 4.79), π-donor hydrogen bond (4.59), unfavorable acceptor-acceptor (5.26)
38	Ile194, Val200, Lys208, Ser209, Val 210	Conventional hydrogen bonds (4.88, 5.48), π-σ (4.80, 5.23), van der Waals (4.36),π-alkyl (4.80, 6.63),

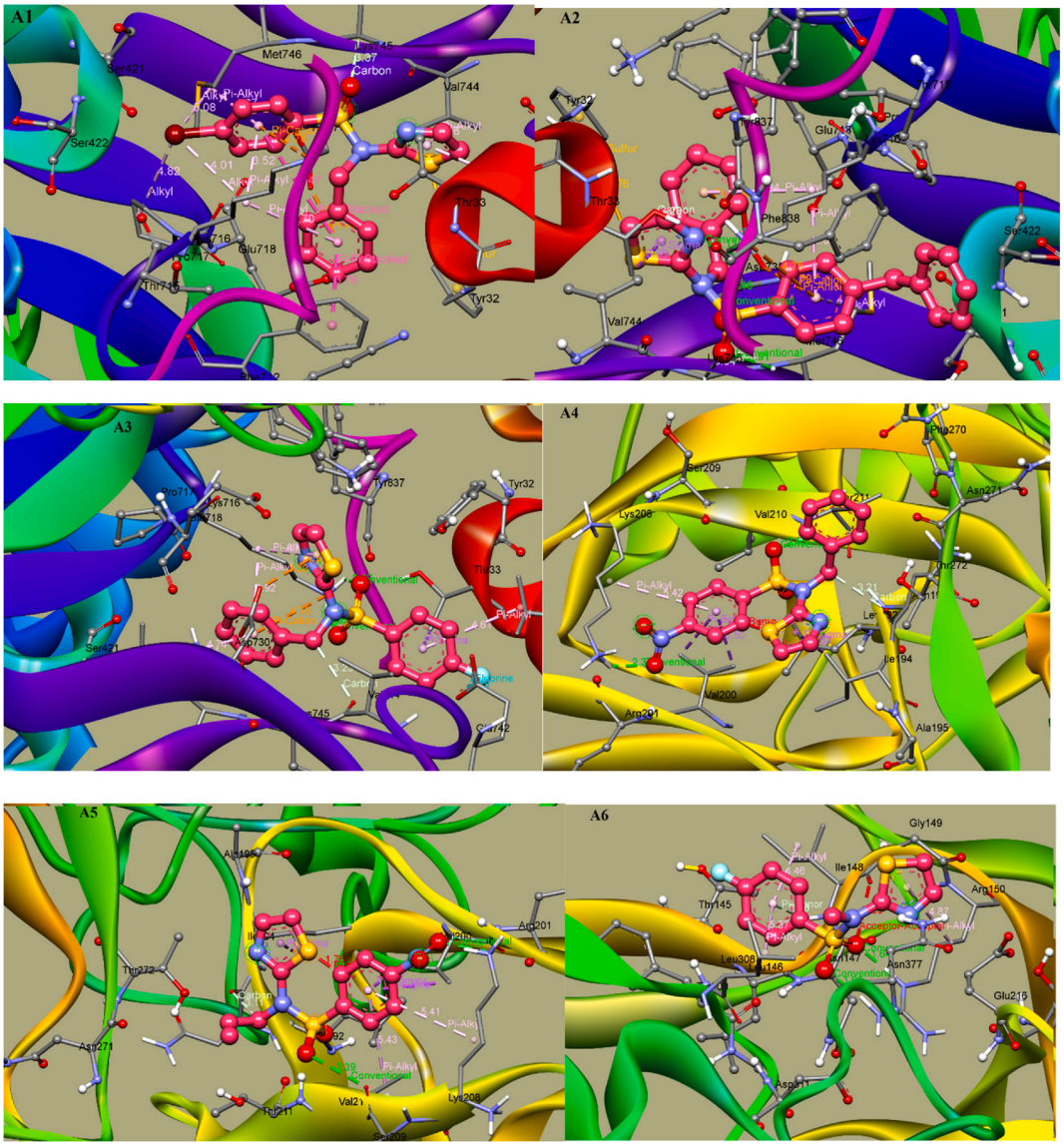

Fig. 4. Three-dimensional representations of the binding pockets of target substrate occupying the ligand molecules **21** (A), **22** (B), **24** (C), **25** (D), **32** (E), and **38** (F) in the protein bound state.

that can adjust to the dynamics of proteins and thus precisely quantifying protein flexibility is crucial in drug research to forecast binding affinity and enhance potential therapeutic options [94]. The complexes of compounds **21** and **24** were analyzed and found little flexibility in the amino acid residues ranging from 0.047 Å for Ser 169 to 0.368 Å for Thr426 with an average value of 0.114 Å for compound **21** and from 0.058 Å for Val 345 to 0.319 Å for Met 241 with an average value of 0.146 Å indicating slightly increased fluctuations for compound **24** and overall, The data unveils the stability exhibited by the ligand-protein complexes (Fig. 6).

3.9.3. Solvent Accessible Surface Area (SASA)

Solvent Accessible Surface Area (SASA) measures the surface area of a biomolecule accessible to solvent molecules, crucial for understanding biomolecular dynamics, especially proteins [95]. It quantifies the exposure of different regions of a molecule to the surrounding solvent, providing information about ligand binding and unbinding events, protein folding and unfolding leading to structural transitions, identification of functionally relevant regions, and interaction of solvent particular water molecules in the real biological systems with the biomolecules [96]. The plots A, B, C, and D in figure represent the SASA profiles of complexes of compounds **21** (blue), **22** (black), and **24** (green) for various portions of protein molecules including the whole protein structure (plot A), backbone (plot B), helix (plot C), and sheet (plot D). Considering the plot A, it is obvious that the complex of compound **21** was buried in the solvent from 32439.38 $Å^2$ to 32797.62 $Å^2$ along the simulation trajectory with minor fluctuations where the solvent interactions were reached to minima of 32369.58 $Å^2$, however, the SASA plot was initiated from 3807.69 $Å^2$, reached to the minima of 3781.33 $Å^2$

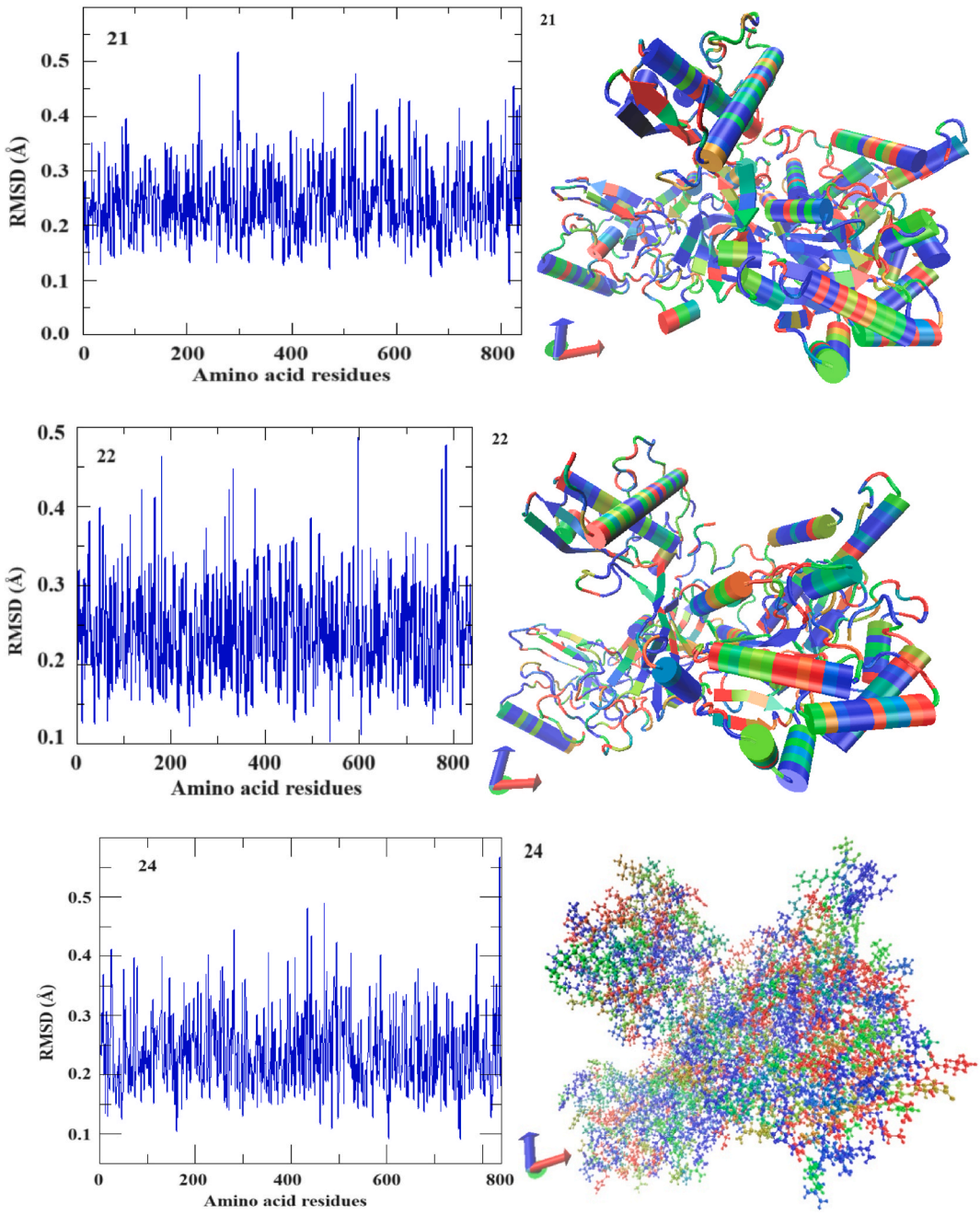

Fig. 5. RMSD plots and color-coded macromolecule structures are shown for ligand-protein complexes of compounds **21** (A), **22**(B), and **24**(C) along with their corresponding color-coded protein structures. (For interpretation of the references to color in this figure legend, the reader is referred to the Web version of this article.)

after 7 ns followed by gradual increase to 3865.06 $Å^2$ at 143 ns and got stabilized. It is also obvious from plot B that the amino acid residues in the backbone of complex were buried in the solvent than the complexes of compounds **22** with the SASA range of 3694.65–3781.01 $Å^2$ and **24** with the SASA range of 3712.50–3794.89 $Å^2$. Considering the interactions of solvent molecules with the amino acids of helix, the complex of compound **21** is surrounded by solvent molecules to the largest extent ranging 8999.46–9141.48 $Å^2$ followed by complex of ligand **22** ranging 8854.06–8974.25 $Å^2$ where the helix of ligand-protein complex of compound **24** offered least surface area accessible to the solvent molecules. Interestingly, the complex of compound **22** offered the greatest surface area of β-sheet to the solvent molecules (Fig. 7). This discussion, along with the figure, illustrates how ligand-protein complexes behave in real cell systems.

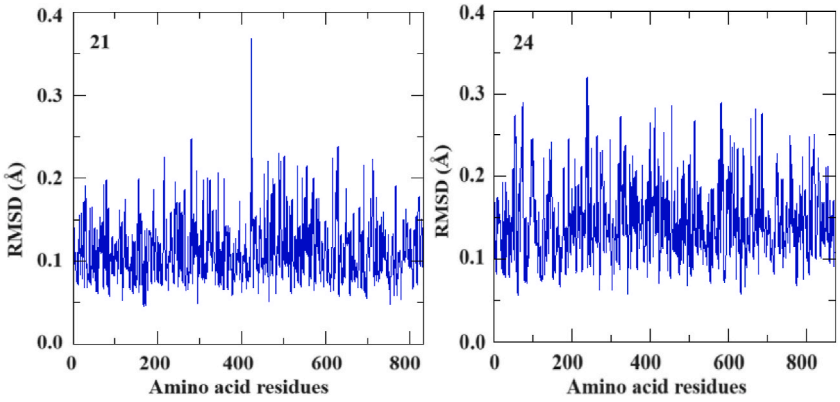

Fig. 6. RMSF plots show protein structure fluctuations in ligand-protein complexes **21**(A) and **24**(B).

4. Conclusion

Twenty-one 2-aminothiazole derivatives were successfully synthesized in an efficient and practical manner; of these, compounds **20**, **21**, **23**, **25**, **27**, **28**, **30**, **31**, and **32** are novel; nevertheless, docking, XRD, and bioactivities increase the overall novelty of the work. The target compounds were characterized using FTIR, NMR, and UV/Vis spectroscopy. In vitro, several substances were discovered to possess antioxidant, anti-urease, and anti-α-glucosidase activities. These molecules are likely to serve as promising motifs for future breakthroughs in the field of drug discovery.Both monoclinic and orthorhombic geometries were seen in the synthesized compounds as was clear through XRD studies of compounds **19**, **23** and **24**. The FMO analysis revealed significant electronic properties of the

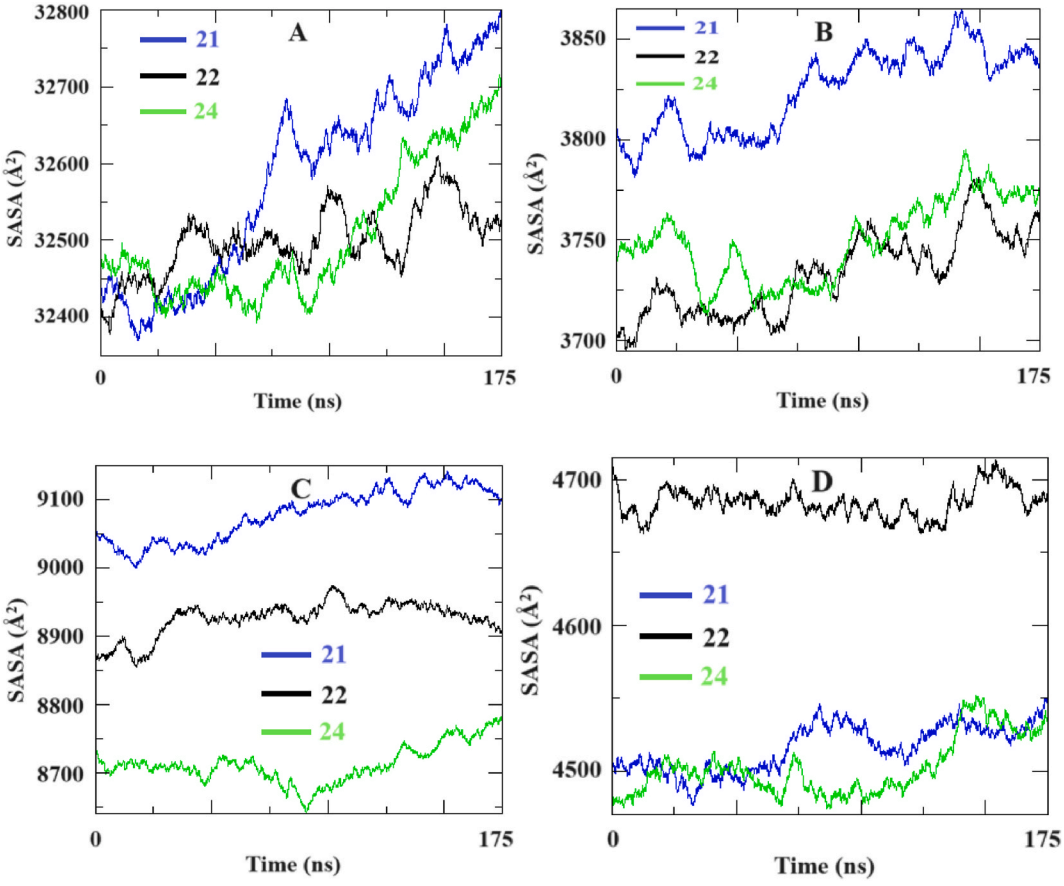

Fig. 7. Solvent Accessible Surface Area (SASA) of protein structures of ligand-protein complexes of compounds **21**, **22**, and **24**, where SASA of whole protein (A), SASA of backbone (B), SASA of helix (C), and SASA of sheet (D).

screened compounds, with HOMO and LUMO energy gaps ranging from 5.805 eV in compound **22** to 0.384 eV in compound **25**, indicating varied reactivity and selectivity. All compounds exhibited high gastrointestinal absorption, enhancing their therapeutic potential, while none crossed the blood-brain barrier, reducing CNS side effects. Optimal skin permeation values (−5.83 to −6.54 cm/s) and QED scores (0.462–0.860) further supported their drug-like properties. Metabolite predictions for compound **21** highlighted diverse transformations, with M5 showing significant analgesic (Pa = 0.784) and anti-inflammatory (Pa = 0.730) activities. Toxicity assessments showed minimal side effects, with ulceration scores near 0.114. Protein binding studies indicated substantial binding efficiencies, with compound **21** forming multiple π-alkyl and π-sulfur interactions, demonstrating strong receptor affinities. These insights provide a comprehensive understanding of the compounds' pharmacokinetic profiles and potential as drug candidates, emphasizing their medicinal chemistry value and guiding future synthetic and clinical explorations.

Funding statement

No specific grant was given for this research by public, private, or nonprofit funding organizations.

Data availability statement

The data will be made available on request.

CRediT authorship contribution statement

Syeda Khair-ul-Bariyah: Writing – review & editing, Writing – original draft, Project administration, Methodology, Investigation, Funding acquisition, Formal analysis. **Muhammad Sarfraz:** Writing – original draft, Visualization, Validation, Software, Data curation. **Muhammad Arshad:** Conceptualization. **Amir Waseem:** Investigation, Funding acquisition. **Hidayat Ullah Khan:** Resources, Methodology, Investigation. **Shahnaz Khan:** Resources, Methodology, Investigation. **Ahsan Sharif:** Writing – review & editing. **Zahoor Hussain Farooqi:** Writing – review & editing. **Ejaz Ahmed:** Writing – review & editing, Writing – original draft, Supervision, Resources.

Declaration of competing interest

The authors declare that they have no known competing financial interests or personal relationships that could have appeared to influence the work reported in this paper.

Appendix A. Supplementary data

Supplementary data to this article can be found online at https://doi.org/10.1016/j.heliyon.2024.e34980.

References

[1] G.M. Badger, The Chemistry of the Heterocyclic Compounds, Academic Press, New York, 1961.
[2] R.H. Wiley, L.C. Behr, R. Fusco, C.H. Jarboe, The Chemistry of Heterocyclic Compounds: Pyrazoles, Pyrazolines, Pyrazolidines, Indazoles and Condensed Rings, John Wiley and Sons, 1967.
[3] M.E. Khalifa, Recent developments and biological activities of 2-aminothiazole derivatives, Acta Chim. Slov. 65 (2018) 1–22.
[4] B.S. Dawane, S.G. Konda, V.T. Kamble, S.A. Chavan, R.B. Bhosale, M.S. Baseer, Multicomponent one-pot synthesis of substituted Hantzsch thiazole derivatives under solvent free conditions, E. J. Chem. 6 (2009) S358–S362.
[5] A. Geronikaki, G. Theophilidis, Synthesis of 2-(aminoacetylamino)thiazole derivatives and comparison of their local anaesthetic activity by the method of action potential, Eur. J. Med. Chem. 27 (1992) 709–716.
[6] C. Papadopoulou, A. Geronikaki, D. Hadjipavlou-Litina, Synthesis and biological evaluation of new thiazolyl/benzothiazolyl-amides, derivatives of 4-phenyl-piperazine, Farmaco 60 (2005) 969–973.
[7] A. Kreutzberger, A. Tantawy, Antibacterial agents. 7. Aminomethinylation of guanidino heterocycles, Arch. Pharm. 314 (1981) 968–969.
[8] M.J. Gorczynski, R.M. Leal, S.L. Mooberry, J.H. Bushweller, M.L. Brown, Synthesis and evaluation of substituted 4-aryloxy- and 4-arylsulfanyl-phenyl-2-aminothiazoles as inhibitors of human breast cancer cell proliferation, Bioorg. Med. Chem. 12 (2004) 1029–1036.
[9] R.N. Misra, H. Xiao, D.K. Williams, K.S. Kim, S. Lu, K.A. Keller, Synthesis and biological activity of N-aryl-2-aminothiazoles: potent pan inhibitors of cyclin-dependent kinases, Bioorg. Med. Chem. Lett. 14 (2004) 2973–2977.
[10] I. Kayagil, S. Demirayak, Synthesis and anticancer activities of some thiazole derivatives. Phosphorus, Sulfur Relat, Elements 184 (2009) 197–207.
[11] A. Göblyös, S.N. Santiago, D. Pietra, T. Mulder-Krieger, J.V. Künzel, J. Brussee, A.P. Ijzerman, Synthesis and biological evaluation of 2-aminothiazoles and their amide derivatives on human adenosine receptors. Lack of effect of 2-aminothiazoles as allosteric enhancers, Bioorg. Med. Chem. 13 (2005) 2079–2087.
[12] P.C. Hang, J.F. Honek, Electronic structure calculations on the thiazole-containing antibiotic thiostrepton: molecular mechanics, semi-empirical and ab initio analyses, Bioorg. Med. Chem. Lett. 15 (2005) 1471–1474.
[13] R.C. Khunt, N.J. Datta, A.R. Parikh, Synthesis and biological evaluation of 5-Oxo-imidazolines and aryl amides, Indian J. Pharmaceut. Sci. 64 (2002) 170–173.
[14] P. Beuchet, M. Varache-Lembege, A. Neveu, J.M. Leger, J. Vercauteren, S. Larrouture, G. Deffieux, A. Nuhrich, New 2-sulfonamidothiazoles substituted at C-4: synthesis of polyoxygenated aryl derivatives and in vitro evaluation of antifungal activity, Eur. J. Med. Chem. (1999) 773–779.
[15] A. Geronikaki, G. Theophilidis, Synthesis of 2-(aminoacetylamino)thiazole derivatives and comparison of their local anaesthetic activity by the method of action potential, Eur. J. Med. Chem. 27 (1992) 709–716.
[16] A. Kreutzberger, A. Tantawy, Antibacterial agents. 7. Aminomethinylation of guanidino heterocycles, Arch. Pharm. 314 (1981) 968–969.

[17] D.S. Prasanna, C.V. Kavitha, K. Vinaya, S.R. Ranganatha, S.C. Raghavan, K.S. Rangappa, Synthesis and identification of a new class of antileukemic agents containing 2-(arylcarboxamide)-(S)-6-amino-4, 5, 6, 7-tetrahydrobenzo [d] thiazole, Eur. J. Med. Chem. 45 (2010) 5331–5336.
[18] C.A. Bolos, K.T. Papazisis, A.H. Kortsaris, S. Voyatzi, D. Zambouli, D.A. Kyriakidis, Antiproliferative activity of mixed-ligand dien-Cu (II) complexes with thiazole, thiazoline and imidazole derivatives, J. Inorg. Biochem. 88 (2002) 25–36.
[19] C.B. Rödl, D. Vogt, S.B. Kretschmer, K. Ihlefeld, S. Barzen, A. Brüggerhoff, J. Achenbach, E. Proschak, D. Steinhilber, H. Stark, B. Hofmann, Multi-dimensional target profiling of N, 4-diaryl-1, 3-thiazole-2-amines as potent inhibitors of eicosanoid metabolism, Eur. J. Med. Chem. 84 (2014) 302–311.
[20] W. Lankes, K. Fleischer, D.C. Gulba, Direktethrombinantagonisten, Herz 26 (2001) S46–S52.
[21] U. Rashid, F. Rahim, M. Taha, M. Arshad, H. Ullah, T. Mahmood, M. Ali, Synthesis of 2-acylated and sulfonated 4-hydroxycoumarins: in vitro urease inhibition and molecular docking studies, Bioorg. Chem. 66 (2016) 111–116.
[22] S. Abbas, H.H. Nasir, S. Zaib, S. Ali, T. Mahmood, K. Ayub, M.N. Tahir, J. Iqbal, Carbonic anhydrase inhibition of Schiff base derivative of iminomethylnaphthalen-2-ol: synthesis, structure elucidation, molecular docking, dynamic simulation and density functional theory calculations, J. Mol. Struct. 1156 (2018) 193–200.
[23] S. Kalra, Alpha glucosidase inhibitors, J. Pakistan Med. Assoc. 64 (2014) 474–476.
[24] R. Subramanian, M.Z. Asmawi, A. Sadikun A, In vitro alpha-glucosidase and alpha-amylase enzyme inhibitory effects of Andrographis paniculata extract and andrographolide, Acta Biochim. Pol. 55 (2008) 391–398.
[25] T. Hatano, H. Kagawa, T. Yasuhara, T. Okuda, Two new flavonoids and other constituents in licorice root. Their relative astringency and radical scavenging effects, Chem. Pharm. Bull. 36 (1988) 2090–2097.
[26] B. Halliwell, Free radicals, antioxidants, and human disease: curiosity, cause, or consequence? Lancet 344 (1994) 721–724.
[27] J. Rowles, M. Olsen, Perspectives on the development of antioxidant antiepileptogenic agents, Mini Rev. Med. Chem. 12 (2012) 1015–1027.
[28] G.J. Kontoghiorghes, C.N. Kontoghiorghe, Prospects for the introduction of targeted antioxidant drugs for the prevention and treatment of diseases related to free radical pathology, Expet Opin. Invest. Drugs 28 (2019) 593–603.
[29] L. Holm, C. Sander, An evolutionary treasure: unification of a broad set of amidohydrolases related to urease, Proteins: Struct., Funct., Bioinf. 28 (1997) 72–82.
[30] C. Follmer, Insights into the role and structure of plant ureases, Phytochemistry 69 (2008) 18–28.
[31] M.J. Maroney, S. Ciurli, Nonredox nickel enzymes, Chem. Rev. 114 (2014) 4206–4228.
[32] H. Mobley, R. Hausinger, Microbial ureases: significance, regulation, and molecular characterization, Microbiol. Mol. Biol. Rev. 53 (1989) 85–108.
[33] H. Mobley, M.D. Island, R.P. Hausinger, Molecular biology of microbial ureases, Microbiol. Mol. Biol. Rev. 59 (1995) 451–480.
[34] C. Montecucco, R. Rappuoli, Living dangerously: how Helicobacter pylori survives in the human stomach, Nat. Rev. Mol. Cell Biol. 2 (2001) 457–466.
[35] C.P. Howson, T. Hiyama, E.L. Wynder, The decline in gastric cancer: epidemiology of an unplanned triumph, Epidemiol. Rev. 8 (1986) 1–27.
[36] D.M. Parkin, F.I. Bray, S. Devesa, Cancer burden in the year 2000. The global picture, Eur. J. Cancer 37 (2001) 4–66.
[37] J. Bremner, Recent research on problems in the use of urea as a nitrogen fertilizer, in: Nitrogen Economy in Tropical Soils, Springer, 1995, pp. 321–329.
[38] R. Newcomer, J. McKee, M. Zanger, Triflic acid–catalyzed rearrangement of unalkylated benzene sulfonanilides, Synth. Commun. 46 (2016) 949–955.
[39] M. Arshad, M. Jadoon, Z. Iqbal, M. Fatima, M. Ali, K. Ayub, A.M. Qureshi, M. Ashraf, M.N. Arshad, A.M. Asiri, A. Waseem, Synthesis, molecular structure, quantum mechanical studies and urease inhibition assay of two new isatin derived sulfonylhydrazides, J. Mol. Struct. 1133 (2017) 80–89.
[40] M.W. Weatherburn, Phenol-hypochlorite reaction for determination of ammonia, Anal. Chem. 39 (1967) 971–974.
[41] Y.I. Kwon, E. Apostolidis, K. Shetty, Inhibitory potential of wine and tea against α-amylase and α-glucosidase for management of hyperglycemia linked to type 2 diabetes, J. Food Biochem. 32 (2008) 15–31.
[42] T. Kulisic, A. Radonic, M. Milos, Inhibition of lard oxidation by fractions of different essential oils, GrasasAceites 56 (2005) 284–291.
[43] H.K. Obied, M.S. Allen, D.R. Bedgood, P.D. Prenzler, K. Robards, R. Stockmann, Bioactivity and analysis of biophenols recovered from olive mill waste, J. Agric. Food Chem. 53 (2005) 823–837.
[44] B. Huang, X. Ban, J. He, J. Tong, J. Tian, Y. Wang, Hepatoprotective and antioxidant activity of ethanolic extracts of edible lotus (Nelumbo nuciferaGaertn.) leaves, Food Chem. 120 (2010) 873–878.
[45] M.C. Sabu, R. Kuttan, Anti-diabetic activity of medicinal plants and its relationship with their antioxidant property, J. Ethnopharmacol. 81 (2002) 155–160.
[46] G. Xiong, Z. Wu, J. Yi, L. Fu, Z. Yang, C. Hsieh, M. Yin, X. Zeng, C. Wu, X. Chen, T. Hou, D. Cao, ADMETlab 2.0: an integrated online platform for accurate and comprehensive predictions of ADMET properties, Nucleic Acids Res. 49 (W1) (2021) W5–W14.
[47] A. Daina, O. Michielin, V. Zoete, SwissADME: a free web tool to evaluate pharmacokinetics, drug-likeness and medicinal chemistry friendliness of small molecules, Sci. Rep. 7 (1) (2017) 42717.
[48] M.F. Sanner, Python. A programming language for software integration and development, J. Mol. Graph. Model. 17 (1999) 57–61.
[49] BIOVIA, Discovery Studio Visualizer. v21.1.0.20298, Dassault Systèmes, San Diego, CA, USA, 2021 (Dassault Systèmes).
[50] J.C. Phillips, D.J. Hardy, D.C. Maia Julio Dc, Scalable molecular dynamics on CPU and GPU architectures with NAMD, J. Chem. Phys. 153 (2020) 044130.
[51] W. Humphrey, A. Dalke, K. Schulten, Vmd – visual molecular dynamics, J. Mol. Graph. 14 (1996) 33–38.
[52] K. Vanommeslaeghe, E. Hatcher, C. Acharya C, CHARMM general force field: a force field for drug-like molecules compatible with the CHARMM all-atom additive biological force fields, J. Comput. Chem. 31 (2009) 671–690.
[53] I.S. Gutiérrez, F.Y. Lin, K. Vanommeslaeghe, Parametrization of halogen bonds in the CHARMM general force field: improved treatment of ligand–protein interactions, Bioorg. Med. Chem. 24 (2016) 4812–4825.
[54] S. Jo, T. Kim, V.G. Iyer Vg, CHARMM-GUI: a web-based graphical user interface for CHARMM, J. Comput. Chem. 29 (2008) 1859–1865.
[55] S. Kim, J. Lee, S. Jo, CHARMM-GUI ligand reader and modeler for CHARMM force field generation of small molecules, J. Comput. Chem. 38 (2017) 1879–1886.
[56] E.W. Bell, Y. Zhang, DockRMSD: an open-source tool for atom mapping and RMSD calculation of symmetric molecules through graph isomorphism, J. Cheminf. 11 (2019) 1–9.
[57] L. Pan, C. Wang, K. Yan, K. Zhao, G. Sheng, H. Zhu, X. Zhao, D. Qu, F. Niu, Z. You, Synthesis, structures and Helicobacter pylori urease inhibitory activity of copper (II) complexes with tridentate aroylhydrazone ligands, J. Inorg. Biochem. 159 (2016) 22–28.
[58] S. Shabana, A. Kawai, K. Kai, K. Akiyama, H. Hayashi, Inhibitory activity against urease of quercetin glycosides isolated from Allium cepa and Psidium guajava, Biosci. Biotechnol. Biochem. 74 (2010) 878–880.
[59] B. Krajewska, W. Zaborska, Jack bean urease: the effect of active-site binding inhibitors on the reactivity of enzyme thiol groups, Bioorg. Chem. 35 (2007) 355–365.
[60] Z.P. Xiao, D.H. Shi, H.Q. Li, L.N. Zhang, C. Xu, H.L. Zhu, Polyphenols based on isoflavones as inhibitors of Helicobacter pylori urease, Bioorg. Med. Chem. 15 (2007) 3703–3710.
[61] E.A. Mohamed, M.J. Siddiqui, L.F. Ang, A. Sadikun, S.H. Chan, S.C. Tan, M.Z. Asmawi, M.F. Yam, Potent α-glucosidase and α-amylase inhibitory activities of standardized 50% ethanolic extracts and sinensetin from Orthosiphon stamineus Benth as anti-diabetic mechanism, BMC Compl. Alternative Med. 12 (2012) 1–7.
[62] G.A. Otunola, A.J. Afolayan, Chemical composition of essential oils obtained from Heteromorphaarborescens (Spreng.) cham. and schltdl leaves using two extraction methods, Sci. World J. (2020) 1–6.
[63] H. Sebai, S. Selmi, K. Rtibi, Lavender (*Lavandula stoechas L.)* essential oils attenuate hyperglycemia and protect against oxidative stress in alloxan-induced diabetic rats, Lipids Health Dis. 12 (2013).
[64] G.R. Gandhi, P. Sasikumar, Antidiabetic effect of Merremiaemarginata Burm. F. in streptozotocin induced diabetic rats, Asian Pac. J. Trop. Biomed. 2 (2012) 281–286, https://doi.org/10.1016/S2221-1691(12)60023-9.
[65] J.L. Chiasson, R. Rabasa-Lhoret, Prevention of type 2 diabetes: insulin resistance and beta-cell function, Diabetes 53 (2004) S34–S38.
[66] O.I. Aruoma, Methodological considerations for characterizing potential antioxidant actions of bioactive components in plant foods, Mutat. Res. 9 (2003) 523–524.

[67] S. Khan, H.U. Khan, F.A. Khan, A. Shah, A. Wadood, S. Ahmad, M. Almehmadi, A.A. Alsaiari, F.U. Shah, N. Kamran, Anti-alzheimer and antioxidant effects of nelumbonucifera L. Alkaloids, nuciferine and norcoclaurine in alloxan-induced diabetic albino rats, Pharmaceuticals 15 (2022) 1205.
[68] S.A. Saeed, M. Zainul, T. Mubarak, Farhad, A. Gila, Antioxidants: their role in health and disease, Int. J. Pharmacol. 1 (2005) 226–233.
[69] J.I. Seeman, Kenichi Fukui, Frontier molecular orbital theory, and the woodward-hoffman rules. Part II. A sleeping beauty in chemistry, Chem. Rec. 22 (2022) e202100300.
[70] N. Ye, Z. Yang, Y. Liu, Applications of density functional theory in COVID-19 drug modeling, Drug Discov. Today 27 (2022) 1411–1419.
[71] M.S. Alqahtani, M. Kazi, M.A. Alsenaidy, M.Z. Ahmad, Advances in oral drug delivery, Front. Pharmacol. 12 (2021) 618411.
[72] S. Gao, E.C. Bell, Y. Zhang, D. Liang, Racial disparity in drug disposition in the digestive tract, Int. J. Mol. Sci. 22 (2021) 1038.
[73] W.M. Pardridge, Drug transport across the blood-brain barrier, J. Cerebr. Blood Flow Metabol. 32 (2012) 1959–1972.
[74] D. Stepanov, S. Canipa, G. Wolber, Huskin DB, a database for skin permeation of xenobiotics, Sci. Data 7 (2020) 426.
[75] C.Y. Jia, J.Y. Li, G.F. Hao, G.F. Yang, A drug-likeness toolbox facilitates ADMET study in drug discovery, Drug Discov. Today 25 (2020) 248–258.
[76] L.R. de Souza Neta, J.T. Moreira-Filho, B.J. Neves, R.L.B. Riveros-Maidana, A.C.R. Guimarães, N. Furnham, C.H. Andrade, F.P. Silva, In-silico strategies to support fragment-to-lead optimization in drug discovery, Front. Chem. 8 (2020) 93.
[77] T. Yamaguchi, Y. Katsuda, T. Hata, N. Miyagawa, K. Arita, Y. Nomura, K. Asahina, Y. Aratsu, M. Kamada, T. Adachi, M. Noguchi, S. Doi, P. Crowe, E. Bradley, R. Steensma, H. Tao, M. Fenn, R. Babine, X. Li, S. Thacher, H. Hashimoto, M. Shiozaki, SAR exploration guided by LE and Fsp(3): discovery of a selective and orally efficacious RORγ inhibitor, ACS Med. Chem. Lett. 7 (2015) 23–27.
[78] G.H. Ta, C.S. Jhang, C.F. Weng, M.K. Leong, Development of a hierarchical support vector regression-based in silico model for caco-2 permeability, Pharmaceutics 13 (2021) 174.
[79] J.D. Irvine, L. Takahasi, K. Lockhart, K. Cheong, J.W. Tolan, H.E. Selick, J.R. Grove, MDCK (Madin–Darby canine kidney) cells: a tool for membrane permeability screening, J. Pharm. Sci. 88 (1999) 28–33.
[80] S. Kalyaanamoorthy, K.H. Barakat, Development of safe drugs: thehERG challenge, Med. Res. Rev. 38 (2018) 525–555.
[81] D.S. Wishart, S. Tian, D. Allen, E. Oler, H. Peters, V.W. Lui, V. Gautam, Y. Djoumbou-Feunang, R. Greiner, T.O. Metz, BioTransformer 3.0-a web server for accurately predicting metabolic transformation products, Nucleic Acids Res. 50 (2022) W115–W123.
[82] A. Hospital, J.R. Goñi, M. Orozco, J.L. Gelpí, Molecular dynamics simulations: advances and applications, Adv. Appl. Bioinforma. Chem 8 (2015) 37–47.
[83] X. Lin, Applications of molecular dynamics simulations in drug discovery. In Advances in Protein Molecular and Structural Biology Methods, Academic Press, 2022, pp. 445–465.
[84] A. Uttarkar, A.P. Kishore, S.M. Srinivas, S. Rangappa, R. Kusanur, V. Niranjan, Coumarin derivative as a potent drug candidate against triple negative breast cancer targeting the frizzled receptor of wingless-related integration site signaling pathway, J. Biomol. Struct. Dyn. 41 (2023) 1561–1573.
[85] B.B. Sokmen, S. Ugras, H.Y. Sarikaya, H.I. Ugras, R. Yanardag, Antibacterial, antiurease, and antioxidant activities of some arylidene barbiturates, Appl. Biochem. Biotechnol. 171 (2013) 2030–2039.
[86] Y. He, K. Liu, F. Cao, R. Song, J. Liu, Y. Zhang, W. Li, W. Han, Using deep learning and molecular dynamics simulations to unravel the regulation mechanism of peptides as noncompetitive inhibitor of xanthine oxidase, Sci. Rep. 14 (2024) 174.
[87] Y. Fu, J. Zhao, Z. Chen, Insights into the molecular mechanisms of protein-ligand interactions by molecular docking and molecular dynamics simulation: a case of oligopeptide binding protein, Comput. Math. Methods Med. (2018) 3502514.
[88] S. AlRawashdeh, K.H. Barakat, Applications of molecular dynamics simulations in drug discovery, in: In Computational Drug Discovery and Design, Springer US, New York, NY, 2023, pp. 127–141.
[89] B. Knapp, S. Frantal, M. Cibena, W. Schreiner, P. Bauer, Is an intuitive convergence definition of molecular dynamics simulations solely based on the root mean square deviation possible? J. Comput. Biol. 18 (2011) 997–1005.
[90] K. Sargsyan, C. Grauffel, C. Lim, How molecular size impacts RMSD applications in molecular dynamics simulations, J. Chem. Theor. Comput. 13 (2017) 1518–1524.
[91] O.M.H. Salo-Ahen, I. Alanko, R. Bhadane, A.M.J.J. Bonvin, R.V. Honorato, S. Hossain, A.H. Juffer, A. Kabedev, M. Lahtel-Kakkonen, A.S. Larsen, Molecular dynamics simulations in drug discovery and pharmaceutical development, Processes 9 (2021) 71.
[92] M. De Vivo, M. Masetti, G. Bottegoni, A. Cavalli, Role of molecular dynamics and related methods in drug discovery, J. Med. Chem. 59 (2016) 4035–4061.
[93] P. Sneha, C.G.P. Doss, Molecular dynamics: new frontier in personalized medicine, Adv. Protein Chem. Struct. Biol. 102 (2016) 181–224.
[94] M.S. Badar, S. Shamsi, J. Ahmed, M.A. Alam, Molecular dynamics simulations: concept, methods and applications, In Transdisciplinarity, Cham: Springer International Publishing 131-151.
[95] N. Okimoto, N. Futatsugi, H. Fuji, A. Suenaga, G. Morimoto, R. Yanai, Y. Ohno, T. Narumi, M. Taiji, High-performance drug discovery: computational screening by combining docking and molecular dynamics simulations, PLoSComput, Biol. 5 (2009) e1000528.
[96] S.J. Fox, J. Li, Y.S. Tan, M.N. Nguyen, A. Pal, Z. Quaray, S. Yadahalli, S. Kannan, The multifaceted roles of molecular dynamics simulations in drug discovery, Curr. Pharmaceut. Des. 22 (2016) 3585–3600.